NUCLEAR ENGINEERING

NUCLEAR ENERGY

NUCLEAR REACTORS

Nuclear engineering is a branch of engineering concerned with peaceful uses of nuclear energy. It includes the study of processes related to the controlled release of fission and fusion energy and the conversion of nuclear energy into other useful forms of energy such as heat and electricity. Significant progress has been made over the past three decades in generating electricity from nuclear fission power plants, while intense research is still underway to achieve controlled release of nuclear fusion energy. We focus our discussion on fission reactor physics and engineering.

In addition to accurate and timely control of the self-sustaining fission reaction in the nuclear reactor core, special attention must be given to the safe removal and efficient utilization of this unique, intense form of energy. Because high-energy ionizing radiations are emitted in the fission process, mechanical and structural properties of materials used in a nuclear power plant may degrade due to radiation exposure during the operating life of the plant. This requires accurate understanding of the mechanisms for interaction of radiation with matter and optimal selection of material compositions and structures for various components in nuclear power plants. Detection and monitoring of different forms of radiation in nuclear power plants forms a key element in the overall effort to ensure safety of the public associated with nuclear electricity generation. Nuclear engineers are also engaged in developing techniques that provide beneficial uses of ionizing radiations in industrial, scientific and medical applications.

NUCLEAR POWER PLANTS

As of March 2006, 104 nuclear power plants provide an installed electrical generating capacity of 101 GW(electric) and account for about 20% of electricity generated in the United States, while 444 nuclear power plants provide an installed capacity of 372 GWe worldwide. All of the nuclear power plants in the U.S. and 80∼85% worldwide utilize light-water cooled reactors (LWRs), which may be grouped (1–3) into pressurized water reactors (PWRs) and boiling water reactors (BWRs). We refer common water as light water, in contrast to heavy water which consists of oxygen and deuteron, the heavy isotope of proton. About 70% of LWRs operating in the U.S. and around the world are PWRs. In the bulk of nuclear power plants, energy released in the fission process is deposited as heat energy initially in fuel pins enclosed in metallic tubes. This energy is eventually transmitted through heat conduction and convection to fluid circulating through the reactor core which is located within a steel pressure vessel. In the case of LWRs, water is used as the circulating fluid, known as the *reactor coolant*. In gas-cooled reactors, pressurized gases, e.g., helium or carbon dioxide, may serve the role of reactor coolant, while circulating liquid metal, e.g., sodium or lead, picks up the heat in liquid-metal cooled reactors (LMRs) (2). The *CANDU* (Canadian Deuterium Uranium) reactor (2) may be cooled either with heavy or light water.

Once the fission energy is picked up by the reactor coolant in the PWR, the coolant circulates through a heat exchanger, where the heat is transferred from the primary loop to the secondary loop, as illustrated (4) schematically in Fig. 1. The heat exchanger is functionally similar to the radiator in an automobile, where the heat produced in the internal-combustion engine is dissipated through a circulating fluid. The heat exchanger in the PWR is known as a *steam generator*, since the circulating fluid in the secondary heat transfer loop is allowed to boil and the resulting steam is separated from liquid. The steam is used to turn the steam turbines and electrical generators, thereby producing electricity. Included in the schematics of Fig. 1 is a *pressurizer*, which is essentially an extension of the primary loop to regulate the pressure of the primary system, and a reactor coolant pump which circulates the reactor coolant. The circulating fluid in the secondary heat transfer loop is known as *feedwater* and the steam that exits from the turbines is condensed into feedwater in the condenser and associated machinery. The condenser as well as the feedwater system is illustrated in Fig. 1. The feedwater system reheats the condensed steam and regulates the temperature of the feedwater before it recirculates into the secondary side of the steam generator. The heat transferred from the steam into the condenser is eventually rejected to the atmosphere through a cooling pond or cooling tower in a tertiary loop, which is the final heat transfer loop shown in Fig. 1.

The reactor pressure vessel, coolant pump, steam generator, and pressurizer are enclosed in a concrete containment structure, built with an inner steel liner. The plant components located within the containment building are collectively known as the *nuclear steam supply system* (NSSS), while those located outside the containment are generally known as the *balance of plant* (BOP). Particular attention is given to the reliability and integrity of NSSS components, which are subject to specific regulations and oversight by the U.S. Nuclear Regulatory Commission. In modern BWRs employing a direct cycle, coolant water circulating in the primary loop is allowed to boil inside the reactor vessel. Steam is separated from liquid water in the reactor vessel and is used to turn the turbo-generators, in much the same way steam extracted from the steam generators in PWRs is used to generate electricity. Incorporation of a direct cycle in BWRs eliminates a heat transfer loop and allows for simplifications in the plant system design. Production of a significant amount of steam within the reactor core, however, requires a number of special considerations for the design and analysis of reactor core and fuel elements in BWRs.

Located inside the reactor pressure vessel of a PWR plant, illustrated (4) schematically in Fig. 2 (a), is the reactor core comprising 150∼200 fuel assemblies, surrounded by steel plates which form the flow baffle. A cylindrical barrel separates the upward flow of coolant through the core from the inlet coolant flowing downward in the an-

J. Webster (ed.), *Wiley Encyclopedia of Electrical and Electronics Engineering*. Copyright © 2007 John Wiley & Sons, Inc.

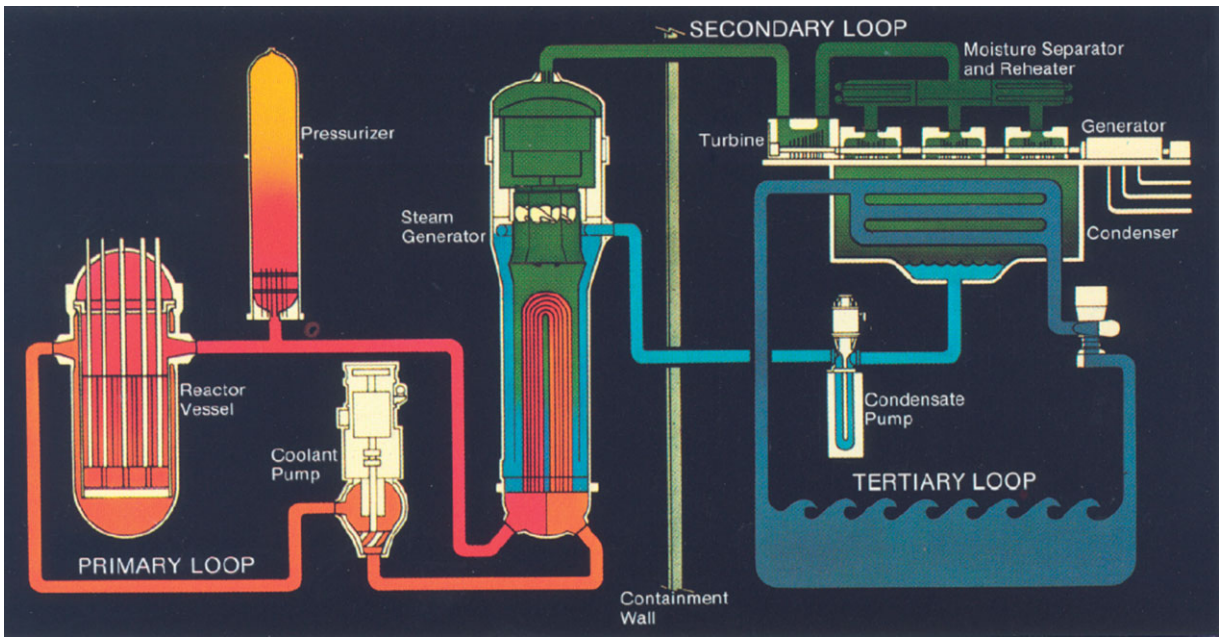

Figure 1. Overall system layout for a PWR plant, indicating key components and illustrating connections between the primary, secondary, and tertiary loops. (Courtesy of Westinghouse Electric Corporation.)

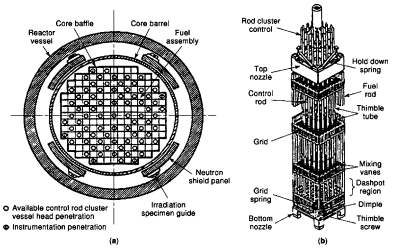

Figure 2. Core and fuel assembly structure of a typical PWR plant. (a) Top view of the reactor core, comprising fuel assemblies and other structures inside the reactor vessel; (b) Sketch of a fuel assembly illustrating fuel rods, spacer grids, rod cluster control elements, and other components. (Courtesy of Westinghouse Electric Corporation.)

nulus formed by the barrel and pressure vessel. Neutron shield panels are located in the lower portion of the vessel to attenuate high-energy gamma rays and neutrons leaking out of the core, thereby reducing the radiation-induced embrittlement of the vessel. Specimens to monitor radiation exposure of the vessel are also indicated in Fig. 2 (a). Figure 2 (b) illustrates a typical PWR fuel assembly, with an array of approximately 250 fuel rods, each consisting of a stack of UO_2 pellets loaded in zirconium-alloy tubes with a diameter of 10∼12 mm and an effective fuel length of 3.6 m. Other prominent structures for the fuel assembly include the spacer grids and clustered control absorbers inserted into the top of the assembly.

NUCLEAR REACTOR PHYSICS

Designing a nuclear reactor core involves the determination of nuclear fuel element configurations (5–7) and mechanical and control devices so that the we may attain a self-sustaining chain reaction, i.e., critical configuration, in the core and produce power over a substantial period of core life without refueling. This entails an initial selection of fuel material, composition, and geometry, together with devices to control the chain reaction, thermal and mechanical structures for fluid flow, heat transfer system, and mechanical support for core components. Equations representing the balance of neutrons undergoing migrations in and out of the core and interacting with fuel and non-fuel materials in the core are solved (5–7) to arrive at an estimate of the critical core configuration with fresh fuel. This stage of design calculations invariably requires iterative adjustments of fuel, fluid, or control configurations until an initial criticality is attained.

A key aspect of the neutron balance equation is the representation of probabilities that neutrons interact with various materials in the core, including the probability that neutrons induce the fission chain reaction in fuel. Since neutrons are electrically neutral, they penetrate the electron orbits of an atom and interact with the nucleus. Thus, neutron interactions with matter entail nuclear reactions and the reaction probability (5,6,8) is expressed in terms of the effective cross sectional area of a given nucleus or simply *nuclear cross section*. The cross section depends heavily on the structure of the nucleus involved, the relative speed between the neutron and nucleus, and the type of reaction, e.g., absorption or scattering collision. The probability of neutrons leaking out of the core also depends on the speed or energy of neutrons. Neutrons are created in the fission process with high energy, typically around 2.0 MeV of kinetic energy on average, corresponding to a speed of 2.0 $\times$ 10^7 m/s. These high-energy neutrons undergo collisions with nuclei of the surrounding material and may either be absorbed by the nuclei or undergo scattering collisions

and emerge with a reduced kinetic energy and speed. The slowing down of neutrons through scattering collisions is known as *moderation* of neutrons and materials comprising nuclei with low atomic weight and small absorption cross section, e.g., light water, heavy water, graphite, and beryllium, are known as *moderators*. Moderators are often introduced in nuclear reactor cores, because the neutron-nucleus reaction probability increases significantly as the neutron speed decreases, and light nuclei are more efficient in reducing the neutron energy through scattering collisions than heavy nuclei. Typically in an LWR core, about 75% of fissions are induced by neutrons of energy below 0.625 eV, often referred (7) to as *thermal neutrons*. Thus, the balance equation or criticality relationship for a reactor core has to account for the slowing down of high-energy neutrons born in the fission process, absorption collisions with the nuclei of incore and excore materials, and leakage of neutrons out of the core as well as the chain reaction process itself.

In a typical fission reaction, 2.45 neutrons are released on average. One of these 2.45 neutrons causes fission in a fuel nucleus to sustain the chain reaction, while the remaining 1.45 neutrons may either be absorbed in non-fission reactions in fuel or in non-fuel materials or may leak out of the core. The ratio of the number of neutrons available in a nuclear reactor core in the present generation of chain reactions to that in the previous generation is known as the *effective multiplication factor* k_{eff}. When $k_{\text{eff}} = 1.0$, the population of neutrons in each generation stays constant and the system is called critical. When $k_{\text{eff}} > 1.0$, the system is supercritical and the neutron population would increase from one generation to the next, while, in a subcritical system with $k_{\text{eff}} < 1.0$, the neutron population will die away given a sufficient period of time. We may write $k_{\text{eff}} = k_\infty P_{\text{NL}}$, where k_∞ is the effective multiplication factor for an infinitely large chain reacting system and is known as the *infinite multiplication factor* while P_{NL} represents the probability that neutrons do not leak out of the chain reacting system of a finite size, e.g., a reactor core. To reduce the leakage of neutrons out of the core, i.e., to increase P_{NL}, the core is surrounded with reflectors comprising moderating materials. The critical mass of a reflected core is therefore smaller than that for a bare, unreflected core of the same composition and layout.

The detailed balance statement describing the time-dependent neutron behavior in a reactor core is obtained as a complex integro-differential equation, known as the *Boltzmann neutron transport equation* <xref target="W5211-mdis-0007"/>. Because of the complexity involved in and computational effort required for solving the transport equation for realistic problems, a series of approximations is usually employed to provide sufficiently accurate estimates for the spatial and energy distributions of neutrons and the criticality of a reactor core. The approximations typically involve the synthesis of detailed solutions for a subregion of the core with approximate global calculations for the entire core.

NUCLEAR REACTOR SAFETY

When a neutron is absorbed in a uranium nucleus and the resulting compound nucleus splits, usually into two fragments, approximately 200 MeV of fission energy is released and carried away by several different types of ionizing radiation, neutrons, and fission fragments or products. The energy density in a nuclear reactor core is six orders of magnitude higher than that typically encountered in conventional, fossil-fueled power plants. This simple fact translates into an important observation that a 1.0-GWe nuclear plant consumes approximately 1.0 Mg of uranium per year compared with approximately 3.0×10^6 Mg of coal consumed in a coal-fired plant of the same capacity. This high energy density in nuclear plants implies that various components in the core will be subject to intense heat and have to be properly cooled and maintained. Degradation of mechanical properties of materials, subject to intense radiation exposure, has to be duly considered in the design and operation of nuclear power plants. Since the majority of the fission products are radioactive, additional energy is released from the decay of fission products, even after the fission chain reaction is terminated. Removal of decay heat is a primary concern in postulated accidents (9) involving loss of cooling. Indeed, in the Three Mile Island accident of 1979, the failure to remove decay heat, long after the fission events were terminated, resulted in meltdown of a significant number of fuel elements in the core.

Most of the risk to the general public due to nuclear energy production is associated with operating nuclear power plants and, to a lesser extent, with the disposal of radioactive waste generated. Since radiation release from normally operating nuclear plants is negligible, public risk associated with nuclear power plant operation is evaluated for postulated accidents. The risk estimates (9, 10) are subject to considerable uncertainties and the perception of nuclear power risks is highly subjective, as is the case for the bulk of our daily activities. We may consider the safety of nuclear power plants as a complex function of the calculated risk and public acceptability of the risk. The acceptability of any risk that we take in our daily life depends heavily on our perception of the risk as voluntary or involuntary and on whether the risk is distributed or acute. This is readily illustrated by the fact that annual traffic fatalities on the order of 50 000 on U.S. highways are simply accepted as a voluntary and distributed risk, while 100∼300 deaths annually resulting from a few airline crashes generate immediate and visible anxiety among the public.

To ensure safe and reliable operation, nuclear power plants are designed with multiple barriers for containing radioactivity generated in the fission process. This concept, known as the *defense in depth*, (9) may be illustrated for LWR cores: (1) UO_2 fuel pellets are in a ceramic matrix retaining fission products, (2) fuel pellets are enclosed and sealed in metallic tubes, (3) fuel elements are located in a steel pressure vessel, and finally (4) the entire NSSS including the pressure vessel, steam generator and pressurizer is located inside a leak-tight containment building. The defense-in-depth approach is used in other system designs and structures whenever possible, together with the

diversity and redundancy in the choice of signals, actuation mechanisms, and equipment for all plant monitoring and control systems. In particular, special attention is given to the design and testing of the reactor shutdown system so that the fission chain reaction in the core may be stopped, under any circumstance, with a high degree of reliability. Similarly, the containment structure is built and tested so that radionuclides released from the NSSS in worst credible accidents, known as *design basis accidents*, may safely be retained. Safe operation of any equipment, however, depends ultimately on human operator and effort is made to provide a high level of operator training and enforce tight regulations and oversight by the U.S. Nuclear Regulatory Commission.

THERMAL AND HYDRAULIC ANALYSIS OF NUCLEAR POWER PLANTS

Determining the outcome and consequences of postulated accidents in nuclear power plants requires computational models that can account for rapid variations in fuel and coolant temperature distributions subject to significant disruptions in the coolant flow. The coupled thermal-hydraulic (TH) analysis (11) has to represent boiling of the reactor coolant for routine operation in BWR cores and in severe transients in PWR cores. A number of sophisticated computational fluid dynamics algorithms have been developed over the years to handle complex nonlinear fluid flow conditions characteristic of the transient reactor TH problems. Some of the well known TH codes include not only discretized first-principles fluid flow models for complex flow circuits in the primary and secondary heat transfer loops but also simplified lumped-parameter models for key power plant components, e.g., the pressurizer and coolant pump.

Detailed TH analysis of the reactor core is very much necessary to obtain accurate estimates of the thermal design margin and to maximize the power output from a given fuel inventory. Because of the high energy density existing in the core, as discussed earlier, we need to determine, to a high degree of accuracy, the spatial distribution of power density in the core and the resulting temperature distributions for fuel elements and reactor coolant. Since there are approximately 40 000∼50 000 fuel rods in an LWR core, it requires considerable computational effort to represent coolant flow explicitly around each fuel rod. Actual TH analysis of reactor coolant channels involves typically detailed solutions for a small region of the core, combined with approximate global solutions for the entire cluster of coolant channels.

SELECTION OF MATERIALS FOR NUCLEAR POWER PLANT COMPONENTS

Various materials (1) used within and outside the nuclear reactor core are subject to intense heat and radiation and may also be exposed to a corrosive environment. Of particular concern is the degradation in physical properties of the reactor pressure vessel, associated internal structures, and coolant piping in the primary loop and small-diameter tubes used in PWR steam generators. Because the integrity of the pressure vessel plays a pivotal role in the overall safety of the plant, special attention is given to the design, material selection, fabrication, testing and inspection of the vessel. Typically, the body of the vessel is low-alloy carbon steel and inside surfaces in contact with primary coolant are clad with a layer of austenitic stainless steel or inconel to minimize corrosion. The primary concern is that fast neutron bombardment may result in slow increases in the temperature, called the nil ductility transition temperature, where the pressure vessel may suffer a significant loss of ductility, and that cooling of the vessel under pressure could develop cracks in the vessel. To minimize the potential problems associated with this *pressurized thermal shock* phenomena, (1) effort has been made in recent years to revise fuel loading patterns and to load dummy fuel elements as additional neutron shields. The possibility of annealing the vessel at radiation-sensitive welds to restore ductility is also under consideration.

Typical steam generators in PWR plants comprise thousands of long tubes, either straight or U-shaped, depending on the type of the heat exchanger design. The steam generators employ a tube-and-shell design, where the radioactive primary coolant flows within the tube and heat is transferred across the tube wall to the non-radioactive feedwater flowing outside the tube in the steam generator shell. Since failure of steam generator tubes provides a leakage path for radioactive nuclides from the primary loop to the secondary side, careful attention is given to the design of the steam generator and selection of the tube material. To minimize corrosion in the secondary side, where water purity is not as strictly enforced as in the primary side, nickel-based alloys, in particular inconel 600, are often used for steam generator tubes in LWRs. Over a period of time, the tubes may develop leaks or cracks due to flow-induced vibrations and high cycle fatigue or due to *stress corrosion cracking*, (1) which results from a combination of mechanical and thermal stress and a corrosive chemical environment. Steam generator tube failures have been reduced through tighter water chemistry control, but PWR steam generators operate with often a number of leaky tubes plugged and a few plants have undergone expensive replacements of the entire steam generator units.

INTERACTION OF RADIATION WITH MATTER

The design and analysis of devices used in industrial and medical applications of radiation as well as of nuclear power plant components requires accurate representation of interactions of nuclear radiation with matter. For nuclear reactor physics analysis, the mechanisms for neutrons undergoing collisions with nuclei of core materials are of primary interest. For the study of radiation shields, interactions of both neutrons and γ-rays have to be accounted for, while the contributions from other ionizing radiations, including β- and α-particles, are minimal and are not considered. Our discussion on radiation interaction mechanisms focuses on neutron reactions, with only a brief review on γ-ray interactions with matter. Charged particle interactions play a major role in plasma physics and

controlled thermonuclear reactions and are not discussed here.

Radioactive Decay

For a sample of any radioactive species or nuclide, the number of particular radioactive nuclei decaying in unit time is proportional (5–8) to the number of the particular radioactive nuclei present at that instant. If $N(t)$ is the number of the particular nuclei existing at t and the decay process is characterized by a proportionality constant λ, known as the decay constant, then the number $-dN$ of the nuclei decaying in time interval dt around t is given by $-dN = \lambda N(t)dt$, or equivalently we write:

$$\frac{dN(t)}{dt} = -\lambda N(t). \tag{1}$$

Given the number $N(0)$ of nuclei of the particular species present at $t = 0$, integration of Eq. (1) yields the number $N(t)$ of the nuclei remaining at time t:

$$N(t) = N(0)e^{-\lambda t}. \tag{2}$$

From Eq. (2), we obtain the *half life* $t_{1/2} = \ln 2 / \lambda = 0.693/\lambda$, defined as the time interval over which the number of radioactive nuclei is reduced to half its initial value, i.e., $N(t_{1/2})/N(0) = 0.5$. The activity of a radioactive substance is defined as λN, in units of either [Bq = 1 disintegration/s] or [Curie = 3.7×10^{10} Bq]. Since Eqs. (1) and (2) hold equally for a sample of unit volume, we consider N, from now on, as the number density of nuclei in units of [nuclei/cm^3].

Neutron-Nucleus Reactions

We consider a simple experiment, where a collimated beam of neutrons of intensity I [neutrons/cm$^2 \cdot$ s] is incident uniformly on a slab of thickness x. The number of neutrons $-dI$ suffering collision in a thin layer dx of the slab per unit area per unit time will be proportional to the beam intensity I and the number Ndx of nuclei in unit cross sectional area of the layer exposed to the beam. With a proportionality constant for the interaction selected as σ, we obtain:

$$\begin{aligned} &-dI = \sigma I N dx, \\ &\text{or alternately,} \qquad -\frac{dI}{I} = \sigma\left(\frac{\text{cm}^2}{\text{nucleus}}\right) N dx \left(\frac{\text{nuclei}}{\text{cm}^2}\right). \end{aligned} \tag{3}$$

The fraction $-dI / I$ represents the fraction of the nominal slab cross sectional area that serves as the effective target area. This leads us to define the reaction probability σ as the *microscopic cross section*, (6, 8) expressed in units of [barn = 10^{-28} m^2], together with the *macroscopic cross section* $\Sigma = N\sigma$, in units of [cm^{-1}]. Equation (3) may be recast:

$$\frac{dI}{dx} = -\Sigma I. \tag{4}$$

In analogy to Eq. (2), we may readily integrate Eq. (4) to calculate the intensity $I(x)$ of the beam of neutrons that penetrate, without suffering any collision, the entire slab of thickness x:

$$I(x) = I(0)e^{-\Sigma x}. \tag{5}$$

Equation (4) suggests that Σ represents the probability of neutron-nucleus reactions per unit distance of neutron travel. For a mixture of materials, Σ has to be constructed as a sum of macroscopic cross sections calculated for constituent nuclides.

The microscopic cross section σ is characteristic (6, 7) of each nuclide and is a function of reaction type, e.g., scattering, capture, fission, and depends heavily on the relative speed between the neutron and nucleus. A nuclear reaction of particular interest involves the formation of a compound nucleus when the neutron is absorbed by the target nucleus. When a compound nucleus is formed, the mass of the nucleus is less than the sum of the neutron mass and target nuclear mass. The compound nucleus is excited to an energy level equal to the sum of the energy corresponding to the mass defect and the neutron kinetic energy. The probability for the compound nucleus formation becomes markedly large when the excitation energy lies near a quantum level of the nucleus. When the compound nucleus (6) decays from the excited state to the ground state with the emission of a γ-ray, the reaction is called *resonance absorption* or *radiative capture*, often written as the (n, γ) reaction. The compound nucleus may also decay with the emission of a neutron in *resonance elastic scattering*. Neutrons with energies $E > 0.1$ MeV may experience *inelastic scattering*, whereby the neutron leaves the compound nucleus in an excited state, which subsequently decays to the ground state with γ-emission. Neutrons may also undergo *potential scattering* with nuclei as though the interacting particles are ordinary billiard balls undergoing elastic collisions. Neutrons may also undergo other types of reactions such as $(n, 2n)$, (n, α), and (n, p) reactions.

One absorption reaction of particular interest is nuclear fission, where the compound nucleus becomes so unstable that it immediately splits into two parts with the release of two or three neutrons. Some nuclides, including ^{233}U, ^{235}U, and ^{239}Pu, allow fission with thermal neutrons and are known as *fissile* nuclides, while *fertile* nuclides, including ^{238}U, need fast neutrons to induce fission. Approximately 200 MeV of energy is released per fission, including the energy recoverable from the radioactive decay of fission products.

Many nuclides, especially those with high atomic number, exhibit a large number of complex and often overlapping resonances. The magnitude of resonance cross sections as well as the energy levels at which the resonances occur depends heavily on the nuclide and neutron cross sections have to be experimentally determined. We illustrate energy dependence of absorption cross section σ_a for ^{238}U in Fig. 3. For scattering collisions, we have to measure not only the magnitude σ_s of the cross section, but also the changes in the energy and direction of neutron travel. For incident neutrons of energy E and direction of motion Ω emerging with energy E' in direction Ω', we determine the *differential scattering cross section* $\sigma_s(E \to E', \Omega \to \Omega')$.

Gamma-Ray Interactions with Matter

Among several different ways γ-rays interact with matter, three mechanisms are of significance to radiation shielding and detection: photoelectric effect, pair production, and Compton scattering. In the photoelectric process, the γ-ray is absorbed by an atom and one of the orbital electrons is ejected from the atom. The photoelectric reaction probabil-

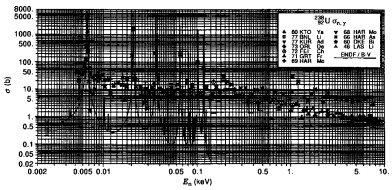

Figure 3. Absorption cross section of ^{238}U plotted as a function of neutron energy. Note a large number of sharp resonances in the range of 6 eV to 150 eV, in particular, those at 6.7 eV, 20.9 eV, and 36.7 eV. (Courtesy of Academic Press, Inc.)

ity is large for low-energy γ-rays, with $E < 1.0$ MeV. In the second type of γ-ray interactions, the photon interacts in the Coulomb field of a nucleus and produces an electron-positron pair. Since the rest-mass energy of two electrons is 1.02 MeV, pair production is possible for photon energy above this threshold and the reaction probability increases rapidly as the photon energy increases further. In Compton scattering, the photon undergoes elastic scattering with an electron and the reaction probability decreases as a function of photon energy. Accounting for all three γ-ray interaction mechanisms, we determine total macroscopic reaction cross sections for γ-rays in much the same way as we define Σ for neutron interactions. By tradition, macroscopic cross sections for γ-ray interactions are called the *attenuation coefficients*, (12) with the symbol μ and in units of [cm^{-1}]. Gamma-ray interaction probabilities are written frequently in terms of the *mass attenuation coefficient* μ/ρ [cm^2/g], where ρ is the physical density of the material. The particular form is often preferred because, for a given photon energy, variations in μ/ρ are small (13) for a variety of materials. Penetration of γ-rays through materials may be estimated through Eq. (5), with Σ replaced by μ. For simple shielding calculations, the uncollided beam intensity calculation of Eq. (5) has to be corrected for multiple photon interactions through an empirical factor, known as the *buildup factor*.

NEUTRON DIFFUSION THEORY

To derive a balance equation for neutrons moving around and undergoing collisions with nuclei of the surrounding medium, we extend Eq. (4) for the rate of neutrons suffering collisions for a collimated beam to the case of neutrons approaching the target in arbitrary directions. Since, for a collimated beam, the beam intensity I may be written as the number density n of neutrons, in units of [neutrons/cm^3], times the speed v of neutrons, we define the *neutron flux* (6, 7) $\phi = n$v, in units of [neutrons/cm^2 · s], where n now represents the number density of neutrons with arbitrary directions of motion. Then, the number of neutron reactions, ΣI, per unit cross sectional area of the slab, per unit time, and per unit distance of neutron travel for the beam may be extended to the reaction rate $\Sigma\phi$ [number of reactions/cm^3 · s] by effectively collecting neutron reaction rates for all possible directions of neutron motion. The scalar flux $\phi = n$v may also be interpreted as the total track length traveled in unit time by neutrons in unit volume regardless of their direction of motion, and remembering that the macroscopic cross section Σ represents the interaction probability per unit distance of neutron travel, we note that $\Sigma\phi$ properly represents the desired reaction rate.

One-Group Neutron Diffusion Equation

In terms of the neutron number density n and flux ϕ, we may now set up a neutron balance equation by writing the time rate of change of neutron population in unit volume as the difference between the rate of neutron production and rate of neutron loss. With the absorption and fission cross sections Σ_a and Σ_f, respectively, together with the average number ν of neutrons produced per fission and the leakage rate written in terms of the current of neutrons $\mathbf{J}$ [neutrons/cm^2 · s], we obtain the balance equation:

$$\frac{\partial n}{\partial t} = \nu\Sigma_f\phi - \Sigma_a\phi - \nabla\cdot\mathbf{J}. \tag{6}$$

Using Fick's law of diffusion $\mathbf{J} = -D\nabla\phi$, with $D = 1/3\Sigma_{tr}$, we rewrite Eq. (6):

$$\frac{1}{\mathrm{v}}\frac{\partial\phi(\mathbf{r},t)}{\partial t} = D\nabla^2\phi(\mathbf{r},t) + (\nu\Sigma_f - \Sigma_a)\phi(\mathbf{r},t). \tag{7}$$

The transport cross section $\Sigma_{tr} = \Sigma_t - \mathring{\mu}_0\Sigma_s$ is not a physical cross section but introduced as a convenient parameter in terms of total cross section Σ_t, scattering cross section Σ_s, and the average cosine of the scattering angle $\mathring{\mu}_0$. Equation (7) is perhaps the most useful form of neutron balance statement and is known as the single-speed or *one-group neutron diffusion equation* (6, 7).

Criticality Condition

For a critical reactor in steady-state operation, we write Eq. (7) as a wave equation:

$$\nabla^2\phi(\mathbf{r}) + B_m^2\phi(\mathbf{r}) = 0, \tag{8}$$

in terms of the *material buckling*, $B_m^2 = \dfrac{\nu\Sigma_f - \Sigma_a}{D}$, which represents the curvature of the flux distribution $\phi(\mathbf{r})$. Standard separation-of-variables techniques yield a general solution to Eq. (7):

$$\phi(\mathbf{r},t) = \sum_{n=0}^{\infty}\psi_n(\mathbf{r})T_n(t). \tag{9}$$

Here, the spatial component of the solution results from an eigenvalue equation:

$$\nabla^2\psi_n(\mathbf{r}) + (B_m^2 + \lambda_n)\psi_n(\mathbf{r}) = 0, \tag{10}$$

with the eigenvalues λ_n, $n = 0, 1, 2, \ldots$, while the temporal solution $T_n(t) = T_n(0)e^{-\lambda_n \mathrm{v} Dt}$ is obtained with the initial condition $T_n(0)$. Equation (10), subject to conditions at the boundary, yields non-trivial eigenfunctions or spatial modes $\psi_n(\mathbf{r})$ only for certain values, i.e., eigenvalues λ_n. If we arrange the eigenvalues in ascending order, we note that, for a reactor to be critical, i.e., for $\phi(\mathbf{r},t)$ to be constant in time, $\lambda_0 = 0$ and all higher harmonics with $\lambda_n > 0$, $n = 1,2,\ldots$, will vanish in short time. This means that, if we obtain the lowest eigenvalue B_g^2 of Eq. (10), corresponding to

the fundamental mode $\psi_0(\mathbf{r})$ with $\lambda_0 = 0$, we should satisfy: (7)

$$B_g^2 = B_m^2. \tag{11}$$

The eigenvalue B_g^2 is determined entirely by the geometry of the system, and hence is known as the *geometrical buckling*. Equation (11) is a succinct statement of criticality of a chain-reacting system: the lowest eigenvalue B_g^2 of the wave equation (10) equals the material buckling B_m^2 defined in Eq. (8). It is also clear that if $B_g^2 > B_m^2$, i.e., $\lambda_0 > 0$, the system is subcritical, and the neutron flux will die away in due time. Likewise, if $B_g^2 < B_m^2$, i.e., $\lambda_0 < 0$, the system becomes supercritical, resulting in an uncontrolled growth of the neutron population.

Equations (8) together with the criticality condition of Eq. (11) yields:

$$\begin{aligned} \frac{\nu\Sigma_f - \Sigma_a}{D} &= B_g^2 \\ \frac{\nu\Sigma_f}{\Sigma_a + DB_g^2} &= 1 = \frac{k_\infty \Sigma_a}{\Sigma_a + DB_g^2} = k_\infty P_{NL} = k_{eff}. \end{aligned} \tag{12}$$

Here, we note that $k_\infty = \nu\Sigma_f/\Sigma_a$ yields the number of fission neutrons produced per neutron absorption and should properly represent the *infinite multiplication factor*. The term DB_g^2 represents the neutron leakage rate relative to the absorption rate represented by Σ_a, and hence P_{NL} represents the *non-leakage probability* of neutrons in the reactor, yielding $k_{eff} = k_\infty P_{NL}$. This is the most direct statement of neutron balance in a multiplying medium expressed in terms of one-group neutron diffusion theory.

Even when the system is not exactly critical, i.e., when $B_g^2 \neq B_m^2$, we may still wish to obtain an expression for the flux $\phi(\mathbf{r})$ as a solution to the eigenvalue equation (10) with the eigenvalue $\lambda_0 \neq 0$ and $\phi(\mathbf{r}) = \psi_0(\mathbf{r})$. Such a solution implies that the material composition and/or arrangement of the reactor should be adjusted until $\lambda_0 = 0$ or $B_g^2 = B_m^2$. Alternatively, we may recast Eq. (10) for $n = 0$ in terms of a multiplicative eigenvalue λ:

$$-D\nabla^2\phi(\mathbf{r}) + \Sigma_a\phi(\mathbf{r}) = \frac{\nu\Sigma_f}{\lambda}\phi(\mathbf{r}). \tag{13}$$

Equation (13) is equivalent to Eq. (10), in the sense that there is an adjustable parameter introduced in either equation. Comparing Eqs. (8) and (13) shows that $\lambda = k_{eff}$ and, when $\lambda \neq 1$, Eq. (13) again implies that the system has to be adjusted until a critical state is attained. Equation (13) is quite useful for non-critical systems, because we are able to obtain solution $\phi(\mathbf{r})$, albeit with $\lambda \neq 1$, and gain understanding of the degree of adjustments required to arrive at a critical configuration. Even without obtaining a precisely critical configuration, we may determine the relative changes in the eigenvalue or *reactivity* of the system due to perturbations in core parameters. Such perturbation calculations would not be possible, without the introduction of the eigenvalue λ in Eq. (13), because it is an eigenvalue equation and renders a unique solution only if the criticality condition $B_g^2 = B_m^2$ is satisfied.

Table 1 presents fundamental mode solutions of Eq. (10), corresponding to $n = 0$, for representative geometries. For a spherical mass of fissionable material, the critical radius R_c of the sphere can be estimated as $R_c = \pi(\frac{D}{\nu\Sigma_f - \Sigma_a})^{1/2}$. The critical radius R_c applies to a bare reactor and, when the fissionable material is surrounded by a reflector, the corresponding critical radius will be less than R_c. We present in Table 2 number densities and microscopic cross sections for a PWR core fueled with UO_2 containing 2.78 wt. % of ^{235}U. We include ^{10}B to represent boric acid dissolved in the coolant at the concentration of 2210 ppm by weight of natural boron in the water. From the data in Table 2, we obtain $\nu\Sigma_f = 0.1570\ cm^{-1}$, $\Sigma_a = 0.1532\ cm^{-1}$, $D = 9.21$ cm, $k_\infty = 1.025$, $B_m^2 = 4.13 \times 10^{-4}\ cm^{-2}$, which yields, for a critical core with height $H = 3.66$ m, $P_{NL} = 0.975$ and effective core radius $R = 1.31$ m. This compares favorably with a more accurate design calculation, $R = 1.22$ m.

Table 1. Flux and Geometrical Buckling for Bare Critical Reactors

Geometry	Flux	Geometric Buckling
Infinite slab of thickness H	$\cos\frac{\pi z}{H}$	$\left(\frac{\pi}{H}\right)^2$
Cylinder of radius R and height H	$J_0\left(\frac{2.405r}{R}\right)\cos\frac{\pi z}{H}$	$\left(\frac{2.405}{R}\right)^2 + \left(\frac{\pi}{H}\right)^2$
Sphere of radius R	$\frac{1}{r}\sin\frac{\pi r}{R}$	$\left(\frac{\pi}{R}\right)^2$
Parallelpiped of sides X, Y, Z	$\cos\frac{\pi x}{X}\cos\frac{\pi y}{Y}\cos\frac{\pi z}{Z}$	$\left(\frac{\pi}{X}\right)^2 + \left(\frac{\pi}{Y}\right)^2 + \left(\frac{\pi}{Z}\right)^2$

Multi-Group Neutron Diffusion Equation

Although one-group diffusion theory provides many useful results both for steady-state and time-dependent behavior of a nuclear reactor, it cannot account for the energy dependence of neutrons as they undergo scattering collisions with core and reflector materials. To remedy this deficiency would require in general representing the slowing down or moderation of neutrons, in terms of the neutron flux and reaction rates varying as an explicit function of the neutron energy. It would be necessary in particular to account for the absorption of neutrons, throughout the slowing down process, in resonances illustrated in Fig. 3. One approximate but practical approach to represent the energy dependence of the neutron population is to discretize the energy variable and establish a neutron balance statement in terms of a number of discrete energy groups (7). We consider a two-group formulation, which provides sufficiently accurate representation of key phenomena of interest in many practical applications.

We set the boundary between the two energy groups so that practically all of fission neutrons are emitted in the first group and the fast neutrons slow down from group 1 to become thermal neutrons in group 2. The source of neutrons in group 2 is entirely due to those escaping absorptions in the fast group and we allow both fast and thermal neutrons to induce the next generation of fissions. For many LWR applications, the group boundary is chosen typically at 0.625 eV. Introducing Σ_r to represent the slowing down of neutrons from group 1 into group 2, we extend Eq. (13) to obtain the *two-group neutron diffusion equations*: (7)

$$-D_1\nabla^2\phi_1(\mathbf{r}) + (\Sigma_{a1} + \Sigma_r)\phi_1(\mathbf{r}) = \frac{1}{k}[\nu\Sigma_{f1}\phi_1(\mathbf{r}) + \nu\Sigma_{f2}\phi_2(\mathbf{r})], \tag{14}$$

$$-D_2\nabla^2\phi_2(\mathbf{r}) + \Sigma_{a2}\phi_2(\mathbf{r}) = \Sigma_r\phi_1(\mathbf{r}). \tag{14}$$

Here we introduce, as in Eq. (13), an eigenvalue $\lambda = k_{eff} = k$ into the fission source term so that we obtain a time-

Table 2. Number Densities and Microscopic Cross Sections for a PWR Core

Nuclide	N (1/b · cm)	σ_{tr} (b)	σ_a (b)	σ_f (b)	υ
H	2.748×10^{-2}	0.650	0.294	0	0
O	2.757×10^{-2}	0.260	1.78×10^{-4}	0	0
Zr	3.694×10^{-3}	0.787	0.190	0	0
Fe	1.710×10^{-3}	0.554	2.33	0	0
^{235}U	1.909×10^{-4}	1.62	4.84×10^{2}	312.0	2.43
^{238}U	6.592×10^{-3}	1.06	2.11	0.638	2.84
^{10}B	1.001×10^{-5}	0.877	3.41×10^{3}	0	0

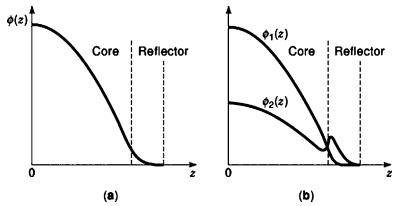

Figure 4. Comparison of one-group and two-group flux distributions for a reflected slab reactor. (a) One-group flux distribution showing a monotonic decrease across the core-reflector interface; (b) Two-group flux distributions, indicating thermal flux peaking in the reflector.

independent balance statement for a reactor which may not be exactly critical.

Provided we generate accurate estimates of the two-group neutron cross sections, including the slowing down cross section Σ_r, Eqs. (14) could account for essentially all of the important aspects of neutron behavior in a chain-reacting system. We illustrate schematically in Fig. 4 two-group flux distributions in a reflected reactor and compare them with the corresponding one-group representation. Fast neutrons produced in the core from the fission process leak into the reflector where they slow down into the thermal group and eventually return to the core to induce further fissions. This point is clearly indicated by the thermal flux peaking in the reflector, with a positive gradient of ϕ_2 at the core-reflector interface. Since the current of neutrons in Eq. (6) is proportional to the negative gradient of flux, this positive gradient of ϕ_2 at the core-reflector interface shows that there is a net current of thermal neutrons back into the core. This aspect of neutron slowing down and migration in a reflected reactor core cannot obviously be accounted for by one-group diffusion theory, which merely indicates, in Fig. 4, a monotonically decreasing flux distribution at the core-reflector interface.

With its ability to provide a much more accurate representation of neutron behavior in a nuclear reactor, two-group diffusion theory naturally provides an improved estimate of the critical mass or the *effective multiplication factor* k. For a bare reactor, we assume the spatial flux distribution for each group is described by the wave equation (10) with a group-independent geometrical buckling B^2, which renders the partial differential equations (14) into a pair of algebraic equations. Dividing the fast-group equation by ϕ_1 and replacing the flux ratio ϕ_2/ϕ_1 in the fission source term by the corresponding expression from the thermal-group equation, we obtain:

$$k = \frac{1}{D_1 B^2 + \Sigma_{a1} + \Sigma_r}(\nu\Sigma_{f1} + \nu\Sigma_{f2}\frac{\Sigma_r}{D_2 B^2 + \Sigma_{a2}}). \qquad (15)$$

For an infinitely large reactor with $B^2 = 0$, Eq. (16) yields:

$$k_\infty = \frac{\nu\Sigma_{f1}}{\Sigma_{a1} + \Sigma_r} + \frac{\nu\Sigma_{f2}}{\Sigma_{a2}}\frac{\Sigma_r}{\Sigma_{a1} + \Sigma_r} \equiv k_1 + k_2, \qquad (16)$$

where we recognize that k_1 and k_2 represent the contributions to k_∞ from fast and thermal neutron fissions, respectively. For a finite reactor, Eq. (16) may be approximated by:

$$\begin{aligned} k &\approx k_\infty \frac{\Sigma_{a1} + \Sigma_r}{D_1 B^2 + \Sigma_{a1} + \Sigma_r}\frac{\Sigma_{a2}}{D_2 B^2 + \Sigma_{a2}} \\ &\equiv k_\infty P_{NLF} P_{NLT} = k_\infty P_{NL}, \end{aligned} \qquad (17)$$

where P_{NLF} and P_{NLT} are the fast and thermal *non-leakage probabilities*, respectively, defined analogously to Eq. (12). The product of P_{NLF} and P_{NLT} yields the net non-leakage probability P_{NL} accounting for the slowing down of fast neutrons and migration of neutrons in both groups.

To amplify the physical interpretation of the two-group expression for k_∞ in Eq. (17), we break up k_2 by introducing the thermal absorption cross section Σ^F_{a2} for fuel:

$$k_\infty = \frac{\nu\Sigma_{f1}}{\Sigma_{a1} + \Sigma_r} + \frac{\Sigma_r}{\Sigma_{a1} + \Sigma_r}\frac{\Sigma^F_{a2}}{\Sigma_{a2}}\frac{\nu\Sigma_{f2}}{\Sigma^F_{a2}} \equiv k_1 + p\ f\eta. \qquad (18)$$

The parameter $p = \Sigma_r/(\Sigma_{a1} + \Sigma_r)$ represents the probability of fast neutrons escaping absorption during slowing down and is called the *resonance escape probability*. The ratio $f = \Sigma^F_{a2}/\Sigma_{a2}$ represents the fraction of thermal neutron absorptions taking place in fuel and is known as the *thermal utilization*, while the last ratio $\eta = \nu\Sigma_{f2}/\Sigma^F_{a2}$ describes the

number of neutrons released per thermal neutron absorption in fuel. Thus, for each thermal neutron absorbed in an infinitely large system, k_2 yields the number of fission neutrons that are emitted, slow down without getting captured in group 1, and finally arrive in group 2. Hence, k_2 represents the contribution to k_∞ from thermal neutron fissions, and will be equal to k_∞ if fast neutrons were not to cause any fission. Setting $\epsilon = 1 + k_1/k_2$, we may interpret ϵ as a fast fission correction to k_2, which would then put Eq. (19) in the form of conventional *four-factor formula* (5). Equation (17) is, however, preferable for LWR analysis where $k_1 \approx k_2/3$. Thus, in this case, ϵ cannot be considered a minor correction for fast fissions, as was the intent when it was first introduced as the *fast fission factor* in the early days of reactor development.

REACTOR KINETICS

To gain quantitative understanding of the dynamic behavior of a nuclear reactor, we now return to the one-group neutron diffusion Equation (7), but with a slight modification to recognize that neutrons are released through radioactive decay of certain fission products as well as directly from the fission process. Hence, a fraction of the neutrons produced in the overall fission process appear with time delays, and they are called *delayed neutrons* while the fission products yielding delayed neutrons are called *delayed neutron precursors*. For ^{235}U fission, the delayed neutron fraction $\beta = 0.0065$ with an effective decay constant $\lambda = 0.08\ \text{s}^{-1}$, averaged over several (usually six) groups of delayed neutron precursors. In terms of the concentration C of delayed neutron precursors, Eq. (7) is now modified to:

$$\frac{1}{\text{v}}\frac{\partial\phi(\mathbf{r},t)}{\partial t} = D\nabla^2\phi(\mathbf{r},t) - \Sigma_\text{a}\phi(\mathbf{r},t) + (1-\beta)\nu\Sigma_\text{f}\phi(\mathbf{r},t) + \lambda C(\mathbf{r},t), \quad (19)$$

coupled with the balance equation for the precursor concentration:

$$\frac{\partial C(\mathbf{r},t)}{\partial t} = -\lambda C(\mathbf{r},t) + \beta\nu\Sigma_\text{f}\phi(\mathbf{r},t). \quad (20)$$

We introduce the approximation that the neutron flux and precursor concentration exhibit the same spatial dependence described by the steady-state equation (13), with geometric buckling B^2, throughout a transient. This yields the *point kinetics equations* describing (7) the time dependence of the neutron number density $n(t)$ and precursor concentration $C(t)$:

$$\frac{dn(t)}{dt} = \frac{K(t)-1}{\Lambda}n(t) + \lambda C(t), \quad (21)$$

$$\frac{dC(t)}{dt} = -\lambda C(t) + \frac{n(t)}{\Lambda}, \quad (21)$$

with the *reactivity* K and *neutron generation time* Λ defined as:

$$K = \frac{k-1}{k\beta}, \quad \Lambda = \frac{\ell}{k\beta}. \quad (22)$$

Here, $k = k_\text{eff}$ defined in Eq. (12), while $\ell = [\text{v}(\Sigma_\text{a} + DB^2)]^{-1}$ represents the average time a neutron spends between its birth and loss due to either absorption or leakage. Both K and Λ are introduced in Eqs. (21) in units of β, and this unit of reactivity is known as dollar. Reactivity is often expressed as $\rho = (k-1)/k$, in units of [% $\Delta k/k$] or in other related units.

Although the point kinetics equations (21) are derived in terms of the neutron number density $n(t)$, we use $n(t)$ conveniently to represent the flux, fission reaction rate, power density or even total power output of the reactor, since anyone of these quantities is proportional to $n(t)$. When $K = 1$ dollar, the reactor is said to be at prompt criticality, which implies that the reactor is able to remain at steady state, even without the help of delayed neutrons. This in turn suggests that, in practice with the delayed neutrons present, the power level will increase exponentially when $K \geq 1$ dollar.

For a step insertion of reactivity K_0, we may obtain solution to the point kinetics equations (21) by applying Laplace transform and solving for the transform $\mathring{n}(s)$ of the power $n(t)$. The transform then is inverted to the time domain to yield two exponential terms with time constants:

$$s_1 \approx \frac{K_0 - 1}{\Lambda} \text{ and } s_2 \approx \frac{\lambda K_0}{1 - K_0}. \quad (23)$$

For a typical LWR configuration with $\lambda = 0.08\ \text{s}^{-1}$ and $\Lambda = 10^{-2}$ s, corresponding to the unnormalized neutron lifetime $\ell = 6.5 \times 10^{-5}$ s, if we introduce a step reactivity $K_0 = 0.5$ dollars, we get $s_1 = -50\ \text{s}^{-1}$ and $s_2 = 0.08\ \text{s}^{-1}$. Similarly, for $K_0 = -1.0$ dollar, we obtain $s_1 = -200\ \text{s}^{-1}$ and $s_2 = -0.04\ \text{s}^{-1}$. These simple examples illustrate that the first exponential term corresponding to s_1 will die away rapidly for reactivity insertions of practical interest and the power level variations, after the initial transients, will be represented by s_2. For $|K_0| < 1$, $s_2 \approx \lambda K_0$, indicating that, for a small reactivity insertion, the e-folding time T of the power level variation is inversely proportional to K_0 to a good approximation. A simple measurement of $T = 1/s_2$, known as the *reactor period*, yields the inserted reactivity K_0. This relationship is known as the *inhour equation* and forms the basis for routine reactivity measurements. Actual applications of the inhour equation, however, require a more accurate expression for T based on six groups of delayed neutron precursors, rather than Eq. (25) with one equivalent group of precursors.

Equation (25) shows that for $K_0 < -1$ dollar, $s_2 \approx -\lambda$, which implies that when a reactor is shut down by inserting a large negative reactivity, the power level cannot decrease, after the initial transients, any faster than with a period $1/\lambda$. In practice, this limiting shutdown period is governed by $T \approx 80$ s, corresponding to the decay constant of the longest-delayed precursor group. Equation (25) indicates further that, for $K_0 > 1$ dollar, i.e., for super-prompt critical transients, s_1 will be positive and large, yielding an exponential increase of power output and essentially requiring no contributions from delayed neutrons. In practice, as the power level increases the fuel and non-fuel materials heat up and reactivity $K(t)$ will decrease due to these temperature increases. The temperature feedback mechanisms are, in fact, an important inherent safety feature of LWRs and will be discussed further in connection with the temperature coefficients of reactivity.

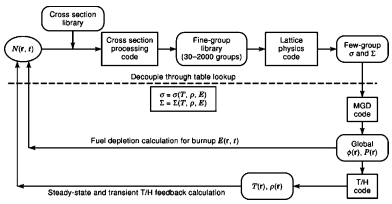

Figure 5. Overall reactor physics calculational procedure, indicating computer codes employed in rectangular boxes and various data or databases in oval or rounded boxes. The coupling between MGD analysis and fuel depletion and T/H feedback calculations is illustrated, together with the cross section parameterization scheme.

REACTOR PHYSICS ANALYSIS AND CORE DESIGN

The *multi-group neutron diffusion* (MGD) equations, as illustrated by the two-group equations (14), are used quite extensively in routine nuclear reactor design tasks. The MGD equations may be solved in full three-dimensional geometry representing individual fuel rods, surrounding structural materials and fluid flow. In many applications of the MGD equations, to lessen the computational requirements, a combination of two-dimensional or one-dimensional calculations may be utilized in a synthesis approach. Regardless of the details represented or the dimensionality retained in the core design analysis, such MGD calculations require macroscopic cross sections for individual materials or subregions of the core. The generation of multi-group cross sections, or *multi-group constants* as they are often called, consists of processing a compiled set of experimental data on neutron cross sections into a suitable discrete group structure, with due account given for the number density of every nuclide specified for the core and reflector regions. Figure 5 illustrates the entire process (14) of generating multi-group constants, including thermal-hydraulic feedback and fuel depletion that have to be incorporated in an overall reactor physics and core design analysis.

Neutron Cross Section Library

The primary source of neutron cross sections currently in use is the Evaluated Nuclear Data File, Part B, Version V or VI (ENDF/B-V or -VI). The ENDF cross section libraries (15–18) are generated by the National Nuclear Data Center (NNDC), located at Brookhaven National Laboratory. The Cross Section Evaluation Working Group monitors activities at the NNDC, which reviews raw cross section data collected in the ENDF, Part A, and compiles into Part B a single set of recommended cross section data in a consistent format. Various NNDC data bases are available for online retrieval. There are a number of other compiled neutron cross section libraries generated at cross section data centers in the U. S. as well as in other countries. The best known among them is the Joint Evaluated File (JEF) maintained (19) at Saclay, France, under the aegis of the Organization for Economic Cooperation and Development (OECD).

The ENDF/B-V library was released around 1979 and is available as a three-volume book (15–17) in a combination of tabulated and curve formats. The publication follows a long tradition of nuclear cross section data published under the Brookhaven report number, BNL-325, and is still informally referred to as BNL-325 or by its nickname *barn-book*. The ENDF/B-VI library was released during the early 1990s and has been implemented in a number of reactor physics or neutronics computer codes. The release of the ENDF/B-VII library is expected before the end of 2006.

Cross Section Processing Codes

As indicated in Fig. 5, the processing of neutron cross section data into a multi-group structure takes two steps. First, the experimental data are processed and averaged over a number of fine-energy groups, where the averaging is performed with a set of approximate estimates of the neutron flux spectrum $\phi(E)$ used as weighting functions over a few broad intervals. For example, $\phi(E)$ is set equal to the energy spectrum $\chi(E)$ of fission neutrons for the neutron energy E in the MeV range and to the Maxwellian distribution $M(E)$ for $E < 1.0$ eV, together with $\phi(E) = 1/E$ for the intervening energy interval. The processed cross section data are then supplied to a lattice physics code, which accounts for the particular composition and geometry of each subregion or fuel assembly and produces microscopic or macroscopic cross sections suitable for global MGD analysis. Among several cross section processing codes available, the NJOY code (20) has gained popularity as a general tool applicable for a number of lattice physics codes. The number of fine groups selected in the processed cross section library varies anywhere between 30 and 2000 groups, depending on the requirements of the lattice physics code that the library is intended for. The fine-group library for the MC^2-2 code (21) would be structured in 2000 groups so that the resonance cross sections and inelastic scattering cross sections of particular interest to LMR lattice physics analysis may be accurately represented.

Lattice Physics Codes

Once a set of fine-group cross sections is generated with an estimate of the space-independent $\phi(E)$ used as a weighting function, we wish to account for the specific composition and geometric details of each fuel assembly and determine the flux spectrum more accurately, which then allows us to collapse the fine-group cross sections into a MGD structure. In traditional *lattice physics analysis*, the entire set of 40 000 $\sim$ 50 000 fuel rods and the surrounding structures in an LWR core is represented by a few representative unit cells each of which comprises a fuel rod and the surrounding moderator. In a *unit cell analysis*, the square lattice is cylindricized and the zirconium-alloy clad is homogenized with the pellet-clad gap. With a large number of identical fuel rods in the core, we assume that there is no net current of neutrons across the cell boundary. This idealized unit-cell construction allows us to determine a cell-average flux spectrum $\phi(E)$, while accounting for the spatial flux distribution across the fuel lattice for thermal neutrons with $E \leq 0.625$ eV and the preferential absorption of fast neutrons in fuel resonances with E in the eV $\sim$ keV range. Each distinct fuel assembly may be represented by one unit cell, typically based on the average ^{235}U enrichment

of the assembly. To account for extraneous materials, e.g., neutron absorbers, structural components, and extra water volumes associated with the instrumentation system, a fourth region, called the *non-lattice region*, is added to the three-region unit cell consisting of the fuel, clad, and moderator regions. This *super-cell arrangement* forms the basis for the well-known LEOPARD code (22) and its variants. Although the LEOPARD code performs, in a strict sense, only a zero-dimensional spectral calculations, it yields sufficiently accurate MGD constants for many LWR configurations and has served as a primary tool for PWR lattice physics calculations for a couple of decades until the late 1980s.

The main limitation of the unit-cell lattice physics methodology lies in its approximate, ad hoc treatment of the non-lattice regions, especially when strong neutron absorbers are present in the region. Removal of this deficiency has resulted in the development of *assembly-level lattice physics codes* which solve an integral form (7) of the neutron transport equation. To derive the integral transport equation for the neutron flux $\phi(\mathbf{r})$ at position $\mathbf{r}$ in a reactor core of volume V, we assume that neutrons emerge isotropically, or equally distributed in all directions, from any fission or scattering event. In terms of the isotropic neutron source $S(\mathbf{r}')$ and the *transport kernel* $T(\mathbf{r}' \rightarrow \mathbf{r})$, which yields the neutron flux at $\mathbf{r}$ due to a unit isotropic source of neutrons at $\mathbf{r}'$, we obtain:

$$\phi(\mathbf{r}) = \int_V d\mathbf{r}' S(\mathbf{r}') T(\mathbf{r}' \rightarrow \mathbf{r}). \tag{24}$$

The transport kernel may be obtained by combining the exponential attenuation of Eq. (5) and the geometric attenuation of the flux of particles, isotropically released at the center $\mathbf{r}'$ of a sphere and arriving at a spherical surface at the radius $|\mathbf{r} - \mathbf{r}'|$:

$$T(\mathbf{r}' \rightarrow \mathbf{r}) = \frac{\exp(-\Sigma_t |\mathbf{r} - \mathbf{r}'|)}{4\pi |\mathbf{r} - \mathbf{r}'|^2}. \tag{25}$$

With Eq. (27) substituted into Eq. (26) and with $S(\mathbf{r})$ written in terms of $\phi(\mathbf{r})$ both for the fission and scattering components, Eq. (26) forms the *integral transport equation*. In practice, the energy dependence has to be explicitly considered for the flux, source, and transport kernel, and the resulting integral equation for the energy-dependent flux $\phi(\mathbf{r},E)$ is discretized both in space and energy. The discretized equation is expressed in terms of the probability that neutrons produced in a subregion of the core will suffer collisions in another subregion. Hence, the integral transport approach to calculate $\phi(\mathbf{r},E)$ is often called the *collision probability* (CP) method.

Although Eq. (26) is derived for an isotropic source $S(\mathbf{r})$, we may account for, with sufficient accuracy, the anisotropy of source neutrons by replacing the total cross section Σ_t in Eq. (27) by the transport cross section Σ_{tr} of Eq. (7). Actual solution of the CP equations for the space- and energy-dependent neutron flux for a two-dimensional representation of distinct material regions in a fuel assembly, however, requires considerable computational effort. Hence, a combination of one- and two-dimensional CP formulations is used in the CPM-3 and CASMO-4 codes (23, 24) for both fast and thermal spectrum calculations at the assembly level. The first step involves a one-dimensional fine-mesh, micro-group calculation, for each of the distinct fuel and absorber rod types. Fine-group fluxes from the micro-group calculations yield macro-group unit-cell average cross sections for each rod in the assembly. This is followed by a two-dimensional CP calculation for the flux distribution using the coarse-mesh, macro-group constants, which represent in (x-y) geometry the actual locations of fuel rods and non-lattice regions of the assembly. The two-dimensional flux distributions are used, together with unit-cell flux distributions, to generate MGD constants averaged over the assembly.

Effects of Material Heterogeneities

Through a synthesis of fine-mesh, fine-group unit-cell calculations and a coarse-mesh, coarse-group assembly calculation, the CP formulations account for material heterogeneities, explicitly and with sufficient accuracy, both at the unit-cell and two-dimensional assembly levels. Material heterogeneities have to be explicitly considered (7) especially when the mean free path of neutrons is comparable to the characteristic dimension of such heterogeneities, as is the case for thermal neutrons in LWR cores. For neutrons in the eV $\sim$ keV range, the resonance absorption of neutrons is affected significantly by material heterogeneities. The thermal utilization f introduced in Eq. (19) has to be modified to represent the spatial flux distribution across the fuel assembly explicitly. Since the absorption cross section of fuel is usually much larger than those for non-fuel materials, thermal neutrons would be preferentially absorbed in fuel, resulting in a lower thermal flux in the fuel region. Since the neutron reaction rate is given by the product of the macroscopic cross section and neutron flux, the fraction f of thermal neutrons absorbed in fuel is reduced in a heterogeneous unit cell compared with that in an equivalent homogenous cell, where the flux distribution is uniform across the mixture of the fuel and non-fuel materials.

Material heterogeneities similarly reduce the absorption of neutrons in fuel in the slowing down range because the neutron flux is depressed in fuel due to large absorption resonances. This, however, renders an opposite effect on k_∞, since reduced resonance absorptions result in a significant increase in the probability that neutrons escape absorption during slowing down, i.e., the resonance escape probability p of Eq. (19). This increase in p, due to fuel lumping, typically exceeds the corresponding decrease in f in LWRs. So was the case in the first critical chain-reacting system built by Enrico Fermi and his colleagues in 1942. In fact, only through a heterogeneous lattice consisting of natural uranium cylinders placed judiciously in graphite blocks, a concept classified during the war, was Fermi able to achieve a critical assembly. This is because a homogeneous mixture of natural uranium and graphite yields $k_\infty < 0.85$ and even an infinitely large assembly comprising such a homogeneous mixture would have remained subcritical.

Overall Reactor Physics Calculation

We may assemble MGD constants generated through the lattice physics analysis for each distinct fuel assembly and

determine flux and power distributions through a global MGD calculation using Eqs. (14) or equivalent. With the power distribution $P(\mathbf{r})$ obtained for a fresh load of fuel elements, we can proceed to calculate the amount of fuel consumed over a period of time. This provides new number densities $N(\mathbf{r},t)$ for fuel nuclides, which are used in a new round of lattice physics and MGD calculations, as illustrated in Fig. 5. We define the fuel burnup (7–25) ΔE over an operating period Δt as a product of power density and Δt, and introduce a relationship between the *fuel burnup* $E(\mathbf{r},t)$, at time t into a fuel cycle, and the time-dependent power distribution $P(\mathbf{r},t)$:

$$\frac{\partial E(\mathbf{r},t)}{\partial t} = P(\mathbf{r},t). \tag{26}$$

The burnup equation (28) is typically integrated over time for each position $\mathbf{r}$ to yield $E(\mathbf{r},t)$ in units of [MWd/kgU] corresponding to the power distribution calculated in units of [MW/kgU]. Likewise, given the power distribution $P(\mathbf{r},t)$, we perform TH calculations to determine the temperature $T(\mathbf{r})$ and density $\rho(\mathbf{r})$ for fuel and non-fuel materials in the core for steady-state analysis or the corresponding time-dependent distributions in transient analysis. The temperature and density data are used to update number densities $N(\mathbf{r},t)$ of every nuclide in the core, requiring another round of lattice physics analysis.

In practical design analysis, the coupling between the lattice physics and MGD calculations, which accounts for both fuel depletion and TH feedback, becomes too costly and unwieldy. A table lookup approach (14, 26) is usually adopted to break up the coupling. Lattice physics calculations are first performed to generate a table of microscopic or macroscopic multi-group constants as a function of a few values of temperature T, density ρ, and fuel burnup E in the expected range of each variable. In MGD calculations, entries in the cross section table are interpolated to yield MGD constants corresponding to specific values of $T(\mathbf{r},t)$, $\rho(\mathbf{r},t)$, and $E(\mathbf{r},t)$ at position $\mathbf{r}$ and at time t, coupled with fuel depletion and TH calculations. In BWR cores, control absorbers are actively utilized during full-power operation and water density varies significantly throughout the core. Hence, for coupled nuclear-thermal-hydraulic (NTH) analysis of BWR cores, special attention has to be given to the cumulative effects of control and water density variations, in addition to the instantaneous values of the control and thermal-hydraulic variables.

THERMAL-HYDRAULIC ANALYSIS FOR REACTOR CORES AND POWER PLANTS

Temperature and density distributions in a reactor core have to be calculated with a high degree of precision to ensure that the reactor operates with a sufficient margin and to properly account for the coupled NTH effects both in steady-state and transient conditions. The axial temperature distribution along the length of a fuel rod is coupled to the radial temperature distribution across the rod radius and to the axial temperature distribution of coolant water in the channel as well as to those in other channels. We assume, however, that the coolant channels are decoupled

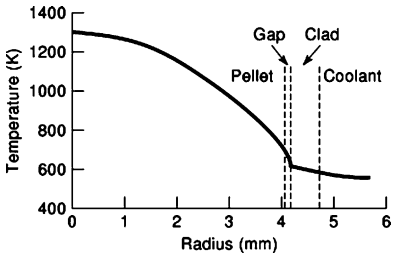

Figure 6. Radial temperature distribution across a fuel rod, illustrating a large temperature drop across the fuel pellet and fuel-clad gap.

from one another and introduce a closed, single-channel model, (7, 11) which corresponds to the unit cell structure considered in the lattice physics analysis. We assume that the rod is infinitely long compared with its small radius and perform a one-dimensional radial temperature calculation for the rod. This is followed by a one-dimensional axial calculation for the coolant temperature distribution in a PWR coolant channel.

Since the temperature rise across a fuel length of 3.6 m in a PWR core is 30∼60 K compared with 600∼1200 K across a radius of 5 mm, it is a reasonable approximation to neglect axial heat conduction in a fuel rod and concentrate on the radial heat conduction. For this one-dimensional heat conduction problem, we assume further that the entire fission energy of 200 MeV/fission is deposited in the fuel rod at a rate of S [kW/m^3] and write the surface heat flux $\mathbf{q}$ [kW/m^2] in term of Fourier's law of heat conduction, $\mathbf{q} = -k\nabla T$, where k is the *thermal conductivity* of the pellet in units of [kW/m · K]. Similar to the steady-state form of the diffusion Equation (6), we obtain the steady-state heat conduction equation:

$$\nabla \cdot \mathbf{q} = S, \text{ or } -k\nabla^2 T = S. \tag{27}$$

Solving Eq. (29) in one-dimensional cylindrical geometry yields $T(r)$ as a quadratic function of radius r. The *linear heat generation rate* P/L, i.e., the power produced per unit length of the fuel rod, is given as a function only of the fuel surface and centerline temperatures, and not of the fuel radius. The overall radial temperature distribution across a fuel rod is illustrated in Fig. 6 for a typical PWR design, showing the temperature variations across the pellet, clad, pellet-clad gap and coolant volume near the fuel rod surface.

For the coolant channel, with coolant mass flow rate W [kg/s], heat capacity C_p [kJ/kg · K], and wetted perimeter M [m], surrounding a fuel rod, we set up a steady-state energy balance for a length Δz of the channel by considering a coolant temperature rise ΔT_c corresponding to surface flux q [kW/m^2] to obtain $WC_\mathrm{p}\Delta T_\mathrm{c} = qM\Delta z$. Here, $WC_\mathrm{p}\Delta T_\mathrm{c}$ represents the energy picked up by the fluid in traversing distance Δz of the channel, which has to equal the heat transferred through the corresponding fuel rod surface area, $M\Delta z$. Rewriting the energy balance as

$$WC_\mathrm{p}\frac{dT_\mathrm{c}(z)}{dz} = Mq(z), \tag{28}$$

and recognizing that $q(z)$ is proportional to the axial power distribution and to the axial neutron flux distribution

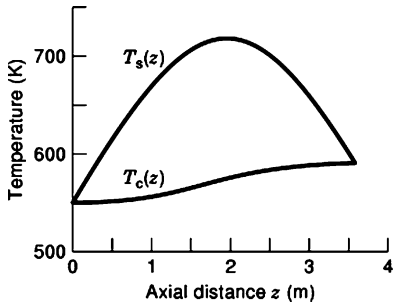

Figure 7. Axial coolant and fuel surface temperature distributions along the length of a typical PWR fuel rod. The coolant temperature $T_c(z)$ is proportional to an integral of the axial heat flux distribution $q(z)$, while the fuel surface temperature $T_s(z)$ is nearly proportional to $q(z)$, adjusted slightly by $T_c(z)$.

$\phi(z) = \cos \frac{\pi z}{H}$ of Table 1, we integrate Eq. (30) for $T_c(z)$ for a channel of length H = 3.6 m, as shown in Figure 7. The axial temperature distribution within the fuel rod follows $q(z)$, adjusted slightly by $T_c(z)$, as illustrated by the pellet surface temperature $T_s(z)$.

For transient TH analysis, (11) the energy balance equations for fuel rods and coolant channels have to be solved together in a fully coupled manner. Such coupled solutions would also be necessary in detailed steady-state TH analysis, often called *subchannel analysis*, (11) where individual fuel rods and coolant channels are discretely represented for subregions of the core comprising several fuel assemblies. The limiting TH conditions in LWR designs entail the design basis accident involving an instantaneous rupture of a primary coolant pipe with a diameter of approximately 1.0 m and the resulting loss of primary coolant. We assume that the severed sections of the pipe are misaligned from each other so that coolant is lost from both sections and that the rupture occurs in the cold leg of the primary piping. This postulated accident scenario (9) is known as the large-break or 200% *loss-of-coolant accident* (LOCA) and serves as the basis for the *emergency core cooling system* (ECCS) design. Since coolant lost from the cold leg cannot pick up any heat from the core, a cold-leg LOCA would result in greater heating of fuel elements and severer damage to the core than a hot-leg LOCA. During a postulated LOCA, ECCS water will be injected through the unbroken pipe into the downcomer annulus between the reactor pressure vessel and core barrel, and will have to counter and quench the steam emerging from the overheated core. In the case of PWR accidents, overheating of steam generators must be also considered in determining the peak temperature and pressure during the accident. Over the past three decades, a number of sophisticated power plant simulation models have been developed to represent complex TH phenomena expected in postulated LOCAs in LWRs. These production TH codes (11, 27) include single- and two-phase fluid flow models of varying degree of complexity and accuracy for a network of flow paths, as well as lumped-parameter models for key plant components, e.g., steam generator and pressurizer. The simplest two-phase flow formulation uses the *homogeneous equilibrium model* (HEM), where the liquid and vapor phases are assumed to be in thermal equilibrium and travel with the same speed, while the more sophisticated *two-fluid models* represent the non-equilibrium thermodynamic conditions and distinct phase velocities of the liquid and vapor phases.

FUEL CYCLE ANALYSIS FOR NUCLEAR POWER PLANTS

Although the main objective of fuel management (25) in any nuclear power plant is to make efficient use of nuclear fuel and to ensure safe, reliable operation of the plant, there are a number of distinct steps that need to be considered preceding and following the production of energy. They are usually grouped into the *front end* of the cycle, including (1) mining of uranium ore, (2) milling and conversion of uranium to suitable forms, (3) isotope enrichment and (4) actual fuel fabrication, and the *back end* of the cycle, including (1) storage of spent fuel, (2) reprocessing and refabrication of fuel and (3) disposal of nuclear waste. In the United States, reprocessing of spent nuclear fuel is not currently performed, but efforts are underway to develop an underground repository for permanent disposal of spent nuclear fuel. The front and back ends of the cycle are also known as excore fuel management in contrast to *incore fuel management*, which will be the focus of our discussion here.

Incore Fuel Management for LWR Plants

Incore fuel management (25) addresses the selection of design and operating parameters that impact nuclear fuel utilization. The placement of fuel rods and control absorbers in fuel assemblies is illustrated in Fig. 2 (b) and loading pattern for fuel assemblies in Fig. 2 (a). Incore fuel management should include the specification of (1) fuel enrichment and control absorber designs, (2) loading pattern for fuel assemblies within the core, (3) cycle length and refueling interval, and (4) overall control requirements and management strategy. LWR fuel designs may call for a uniform fuel enrichment for every rod in a fuel assembly or enrichment varying within an assembly. In BWR assemblies, there are variations in the loading of control absorbers admixed with fuel over the axial length of a given rod as well over different rod locations within an assembly. The control absorbers, known as *burnable absorbers*, are loaded into LWR fuel assemblies to control the reactivity swing associated with fuel depletion and to flatten the core power distribution. The fuel assemblies are typically loaded in a modified checkerboard pattern, with fresh fuel assemblies loaded mostly near the periphery of the core. Selection of these design features and fuel management strategy is dictated primarily by the desire to flatten the power distribution throughout the core, thereby minimizing the peak fuel temperature and maximizing power output. Typically, LWR cores operate with a cycle length, or the time interval between refueling operations, ranging anywhere between 12 to 24 months. At each refueling, one third or fourth of fuel elements are discharged, fuel elements shuffled, and new elements loaded. Recently, increased attention has been given in fuel design and loading strategy to minimize the neutron exposure of the pressure vessel and thereby reduce the degradation of the critical protection barrier in nuclear power plants.

Alternate Fuel Cycles

Currently, all LWRs in the United States operate with a once-through cycle based on UO_2 fuel containing approximately 3 ~ 5 wt. % of ^{235}U. Through radiative capture or (n, γ) reaction, ^{238}U is converted to ^{239}Pu and other Pu isotopes during the reactor operation. Spent nuclear fuel can be reprocessed to recycle the plutonium in the form of $(U\text{-}Pu)O_2$ fuel, known as the *mixed oxide* (MOX) fuel. A number of countries, in particular, France and Japan, have made extensive use of the MOX fuel in LWRs, thereby reducing the burden associated with spent nuclear fuel disposal and extracting extra energy out of the spent fuel. In addition to this basic uranium cycle, limited utilization has been made of alternate cycles involving Pu-U and U-Th fuel. In an LMR core, where liquid metal, e.g., sodium, serves as coolant, the neutron flux spectrum stays hard, i.e., the bulk of fissions occur with high energy neutrons, thereby allowing for an efficient conversion of ^{238}U to Pu isotopes. An LMR core may produce more fissile plutonium, ^{239}Pu and ^{241}Pu, than it consumes, and such a reactor is known as a *breeder*. In yet another alternate fuel cycle, ^{232}Th may be used as fertile material producing fissile ^{233}U. In the Th-U cycle, the production of Pu nuclides may be reduced compared with traditional once-through LWR uranium cycle. This feature could alleviate concerns regarding potential proliferation of nuclear weapons associated with plutonium recycling in LWRs and has contributed to recent resurgence of interest in the Th-U cycle.

Estimation of Fuel Burnup

As defined in Eq. (28), fuel burnup E [MWd/kgU] is calculated as a parameter proportional to the energy produced in fuel. Recognizing that approximately 200 MeV of energy is released per fission and 1 gram atom of U, weighing 0.238 kg, contains 6.022×10^{23} U atoms, equal to Avogadro's number, we obtain E (MWd/kgU) = 939 *fima*. Here, *fima* is defined as the number of *fissions per initial metal atom*, with the word metal referring to heavy metal or actinides, i.e., nuclides with atomic number $Z \geq 89$. For an LWR fuel cycle, *fima* may be written as a product of *fifa*, the number of *fissions per initial fissile atom*, and the enrichment e of fissile ^{235}U. If we introduce F representing the ratio of the total number of fissions to that occurring in the initial fissile ^{235}U atoms and determine the fraction β of initial ^{235}U atoms fissioned, then $fifa = F\beta$, yielding E (MWd/kgU) = 939 $fifa \times e$ = 939 $\beta F e$. An LWR fuel element with e = 0.045 is discharged with β = 0.8, and 45% of fissions occur in Pu, averaged over a cycle, or F = 1.8, which yields *fifa* = 1.45, *fima* = 0.065, and E = 60 MWd/kgU. This fuel burnup corresponds to an LWR fuel batch, discharged after 4.5 years of irradiation time. This simple analysis with *fima* $\approx$ 0.065 also implies that approximately 6.5% of initial fuel loaded may undergo fission and produce energy in LWR cores. This may be contrasted with values of *fima* as large as 0.15 achievable in LMR designs utilizing (U-Pu-Zr) metallic fuel, indicating clearly that LMR designs, even without fuel reprocessing and recycling, could make significantly increased utilization of fuel resources.

RADIOACTIVE WASTE DISPOSAL

Radioactive waste generated during the operation of a nuclear power plant and related fuel cycle activities is generally grouped (28) into high-level waste (HLW) and low-level waste (LLW). Another group of radioactive waste containing transuranics (TRUs), i.e., nuclides with atomic number $Z > 92$, has accrued from the weapons program. The HLW refers to spent nuclear fuel or highly radioactive material resulting from fuel reprocessing, while LLW comprises contaminated clothing, tools, chemicals and liquids that become radioactive during various phases of nuclear power plant operation and from medical procedures. The main concern behind radioactive waste disposal is the presence of long-lived radionuclides in spent nuclear fuel, although due care must also be taken to dispose of LLW as well.

A 1.0-GWe LWR plant operates with a fuel inventory of approximately 100 Mg, with one third of fuel discharged and reloaded every 18 months. For an initial fissile enrichment of 4.5 wt. % of ^{235}U, the discharged fuel contains approximately 1 wt. % of ^{235}U remaining and 1 wt. % of TRUs produced during the fuel lifetime. Plutonium makes up about 90 % of TRUs, with the remaining 10 % comprising minor actinides, Am, Np, and Cm nuclides. Primary nuclides of concern in disposal or storage of unprocessed spent nuclear fuel are actinides ^{239}Pu, ^{240}Pu, ^{237}Np, ^{241}Am, and ^{243}Am, plus fission products ^{99}Tc, ^{129}I, and ^{135}Cs. For underground disposal of spent nuclear fuel, the risk these nuclides pose to the public should be analyzed in terms of the radioactive half life, radiation exposure or dose associated with the particular type and energy of radiation released, and dissolution and transport properties of the species.

With 104 LWRs operating in the U.S., the inventory of spent fuel accumulated by 2010 is expected to be 63 000 Mg. This inventory of fuel would occupy a volume roughly equal to a football field with a depth of 3 m, although actual disposal would, of course, require a much larger space to allow for proper heat dissipation and engineered barriers. Current plans for HLW disposal focus on the underground repository under study at Yucca Mountain, in the vicinity of the Nevada nuclear weapons test site. Studies (29) have been made to explore the feasibility and advantage of reprocessing spent nuclear fuel as well as recycling and transmuting actinides and fission products in critical and subcritical reactor cores. Reprocessing is expected to improve the waste form so that public risk associated with spent fuel disposal will be reduced. Spent fuel recycling for the purposes of waste disposal appears quite promising especially in the hard neutron spectrum of LMR cores but will require further engineering study. Argonne National Laboratory has been developing pyroelectric techniques, (30) which are similar to common elecrorefining process, to reprocess metallic and oxide nuclear fuel. More recently, significant effort has been made to develop the UREX+ aqueous separation and reprocessing processes (31). The pyroelectric and UREX+ processes do not allow the separation of plutonium from highly radioactive fission products or other transuranic materials during the entire reprocessing steps, thereby minimizing proliferation risk associated with spent nuclear fuel reprocessing.

Approximately 100∼200 Mg of LLW, amounting to 500∼1000 m^3 in volume, is generated annually in a 1.0-GWe LWR plant. Considerable premium is placed on decreasing the volume of LLW, both to reduce storage space and disposal charges. Volume reduction of LLW up to a factor of 10 may be achieved through a number of techniques including compaction, evaporation, and incineration. The processed LLW is stored in above-ground facilities, either in the form of covered trenches or tumulus. Considerable effort will, however, be required in the future to clean up and manage mixed chemical-nuclear waste, including the TRU waste, from the nuclear weapons program.

PROBABILISTIC SAFETY ANALYSIS OF NUCLEAR POWER PLANTS

Safe and reliable operation has always played the most important role in the design and analysis of nuclear power plants, as exemplified by multiple safety features and barriers installed to minimize the probability of accidents and the release of radioactive materials to the environment. Since it is not, however, possible to guarantee, under all circumstances, the operability of even highly reliable components, a probabilistic approach, (10) known as *probabilistic risk assessment* (PRA), has been developed to estimate the risk associated with the failure of plant systems and components. Any estimates of such risk, usually calculated in terms of acute and chronic fatalities, are, however, subject to considerable uncertainties. Thus, PRA estimates of the risk due to operating a nuclear power plant should be considered primarily (1) to see if the calculated risk appears acceptable, (2) to compare the risk of operating the plant with that of alternate energy sources or other nuclear plants, and (3) to determine if improvements in plant design or operating strategy should be made.

The PRA technique (10) makes a combined use of two semi-pictorial constructs, called *fault* and *event trees*, to estimate the probability of occurrence of rare events representing the failure of components with high reliability. An event tree follows a sequence of events starting from initiating failures through stages of safety systems to be activated or processes to be invoked, with a success-failure binary branch constructed at each stage. Summing up the probabilities associated with risk-significant sequences yields the overall risk of the system. The probability of failure at each branch point is calculated with a fault tree, which represents in Boolean logic the structural relationship between the failure of the system at the branch, considered the top event of the tree, and components making up the system. The component failures are treated as basic events of the tree contributing to the top event. Given the probability of each basic event, the determination of cutsets, i.e., the set of basic events which causes the top event to occur, and Boolean elimination of any redundancies between the cutsets yield the probability of the top event, supplying the desired branch probability to the event tree. Uncertainties in basic event probabilities, which are difficult to estimate for highly reliable components, are directly reflected in the top event probabilities and, eventually through the event tree, also in the risk calculated for the entire system.

A pioneering application of the PRA technique was made in the 1970s to assess the risk of operating one PWR and one BWR plant, which were intended to serve as surrogates for the entire population of U.S. nuclear power plants. The study (32), published as a U.S. Nuclear Regulatory Commission report, WASH-1400, provided many valuable insights to nuclear power plant safety. In particular, WASH-1400 indicated that the probability of large-break LOCAs is rather small but that small-break LOCAs are much more likely to occur. This particular point was, in some way, validated only a few years later by the Three Mile Island accident (9) of 1979, which indeed was initiated as a small-break LOCA due to a valve failure. In this unfortunate accident, due to incorrect diagnosis of the valve failure, operators turned off, during a critical period, the ECCS system which had been activated automatically as designed. This operator action resulted in meltdown of a large portion of the core but with insignificant release of radioactivity to the environment.

Following the catastrophic Chernobyl accident of 1986, which resulted from flagrant violations of safety procedures and basic design deficiencies, Nuclear Regulatory Commission initiated a study (33) to determine the risk due to severe accidents in nuclear power plants. Included in the study was a comprehensive application of PRA techniques to five representative LWR plants, three PWRs and two BWRs, in the United States. Severe accident risk for each plant was determined by summing the product, (probability of accident) $\times$ (consequences of the accident), for all accidents leading to radiation release to the environment. Figure 8 shows that the accident probability is further broken down into the probability $P(I)$ of initiating events, conditional probability $P(D \mid I)$ of initiating events leading to core and plant damage, and the conditional probability $P(A \mid D)$ of plant damage states leading to containment failures grouped in accident progression bins. The consequences of accident are calculated by sequentially calculating the amount $P(S \mid A)$ of radionuclides released given containment failures and the health consequences $P(C \mid S)$ associated with the radionuclide release. Each of the square boxes in Fig. 8 represents a set of event tree analyses, while the rounded boxes indicate event probabilities or consequences calculated through the event tree analyses. The severe accident risk study, released as NUREG-1150, has provided voluminous documentation on the characteristics and consequences of severe accidents, especially core meltdown accidents. The study suggests that the overall risk of operating the five representative plants is acceptable but that individual plant characteristics, rather than generic attributes, have to be specifically considered in risk studies. The uncertainties in the risk estimates are still quite large, especially because some of the failure probabilities used in the PRA study are determined through subjective expert judgment. One interesting illustration of general usefulness of PRA studies is the identification of a BOP system deficiency in the Zion PWR plant, which was promptly corrected even before the final NUREG-1150 report was released.

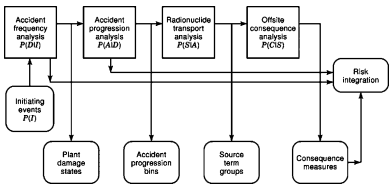

Figure 8. Event tree structure of the NUREG-1150 PRA study, indicating sequential event tree analysis in square boxes, each of which represents the calculation of a conditional probability or consequence. Rounded boxes indicate event probabilities or consequences calculated in the PRA methodology.

INSTRUMENTATION AND CONTROL SYSTEMS IN NUCLEAR POWER PLANTS

Monitoring and controlling core reactivity is one of major tasks in nuclear power plant operation. It is equally important to monitor and control the power distribution in the core so that safety margins are not compromised. We describe the principles of operation of representative radiation detectors, with emphasis on neutron detectors, and discuss how they are used in the nuclear instrumentation system to monitor the core reactivity and neutron population. The reactivity control system in a nuclear power plant handles long-term reactivity variations due to fuel depletion as well as those associated directly with power level changes.

Nuclear Instrumentation System

All devices that detect and measure ionizing radiation rely (34) on converting products of radiation interaction in the detector volume into an electrical signal. For each γ-ray interaction with gas or solid material in the detector volume, a free election and an ion are produced, and the movement of this ion pair in an applied electrical field is converted into electrical current. Neutrons are detected by means of charged particles that are released as a result of neutron interactions within the detector volume. Detection of slow or thermal neutrons makes use of α-particles released through neutron absorption in ^{6}Li or ^{10}B. Through elastic scattering collision with fast neutrons, hydrogen nuclei, i.e., protons, acquire part of the neutron energy and the measurement of these recoil protons provides the desired signal for fast neutrons. Among a variety of neutron detectors using these basic approaches, gas-filled detectors are employed extensively in both incore and excore nuclear instrumentation systems in power plants, because they respond over a wide range of radiation intensity and offer sufficient resistance to radiation damage. Another type of detectors unique to neutron detection is the self-powered neutron detectors (SPNDs), in which electrons produced, either directly or indirectly, in neutron interactions with emitter materials are collected without applied electric field.

To provide continuous power level monitoring, both PWRs and BWRs use a set of neutron detectors covering broad power ranges but with different arrangements: PWR plants rely extensively on BF_4-filled excore detectors in contrast to miniature incore fission detectors installed in BWR plants. Depending on the power level, excore neutron detectors with different designs and characteristics are selected in the PWR instrumentation system to provide the necessary level of discrimination against the gamma background. Fission chambers used in the BWR system are gas-filled detectors which are lined with highly enriched uranium to increase the ionization current and thereby to enhance discrimination against the gammas. In a number of PWR plants, SPNDs, instead of fission chambers, are installed as part of the incore power distribution monitoring system. Fixed neutron detectors provide continuous information both on the core power distribution and power output. Movable fission chambers are employed to perform periodic calibrations of fixed incore and excore neutron detectors in LWR plants.

Reactivity and Power Distribution Control

Core reactivity $K(t)$ defined in Eq. (24) in terms of k_{eff} cannot be measured directly and has to be derived from the measurement of power level variation $n(t)$. Given $n(t)$, we may determine $K(t)$ either through the inhour equation or by inverting the point kinetics equations (21) for $K(t)$. Since the response of a neutron detector is affected by the proximity of the source of reactivity perturbations, e.g., control rod movement, due care must be taken to ensure that the detector reading provides an accurate measure of the core-average neutron flux variation. For this reason, the point kinetics equations (21), derived with the assumption that the spatial flux distribution does not vary during a transient, have to be replaced by the time-dependent MGD equations, essentially combining Eqs. (14) and (20).

Reactivity control in a nuclear power plant has to address short-term reactivity variations associated with power level changes, including emergency reactor shutdowns, and long-term effects due to fuel depletion and fission product buildup. The core power distribution has to be controlled and maintained so that the limitations (25) on peak fuel temperature or surface heat flux are not violated anytime during the operation. In BWR plants, control blades inserted from the bottom of the core are responsible for the bulk of the reactivity and power distribution control tasks. Judicious control of the coolant mass flow rate is also used to vary vapor mass distributions throughout the core and complements the control absorber movement in performing the control tasks. The reactivity and power distribution control tasks in PWR plants are handled through a combination of control rod movement and variation in the concentration of boric acid dissolved in coolant water. Although control rods are exercised during power level variations, the rods are kept essentially all the way out of the core during rated power operation. The reactivity control requirements associated with fuel depletion and fission product buildup are reduced, in both PWR and BWR plants, by the use of burnable absorbers, either in the form of lumped neutron absorbers or absorber materials admixed in fuel.

TEMPERATURE COEFFICIENTS OF REACTIVITY AND INHERENT REACTOR SAFETY

Among the many safety measures built into every operating nuclear reactor is an inherent safety feature associated with the temperature or power coefficients of reactivity. *Reactivity coefficients* (7) refer to changes in reactivity due to changes in power level or fuel and coolant temperatures, and every operating reactor should be designed so that an inadvertent increase in power level will not cause an uncontrollable increase in reactivity. All LWRs operating in the United States and those designed according to U.S. technology all abide by this basic principle. One exception to this basic safety philosophy perhaps was the ill-fated Chernobyl reactor, where one particular reactivity coefficient, known as the void coefficient of reactivity, did not obey this fundamental guideline.

Temperature Coefficients of Reactivity

We invoke the two-group diffusion theory expression of Eq. (19) and approximate the core material as a mixture and fuel and moderator to discuss key factors that control the reactivity coefficients in LWRs. In terms of the reactivity $\rho = (k - 1) / k = \Delta k / k$, we write the power coefficient of reactivity α_p for PWRs in terms of the *fuel temperature coefficient* α_f and *moderator temperature coefficient* α_m:

$$\alpha_p = \frac{\Delta k/k}{\Delta P} \approx \frac{\partial \ln k}{\partial T_f}\frac{\partial T_f}{\partial P} + \frac{\partial \ln k}{\partial \rho_m}\frac{\partial \rho_m}{\partial T_m}\frac{\partial T_m}{\partial P} \equiv \alpha_f \frac{\partial T_f}{\partial P} + \alpha_m \frac{\partial T_m}{\partial P}. \quad (29)$$

We recognize here that a power level variation ΔP affects the reactivity through changes in fuel temperature T_f and moderator temperature T_m and that T_m influences k primarily through thermal expansion of water and the resulting change in water density ρ_m. For the ceramic UO_2 fuel in LWRs, in the case of an increase in T_f, the bulk of the reactivity change is due to increased absorption in fuel resonances, known as Doppler broadening of resonances, with only minor contributions from thermal expansion of fuel. This ensures that the fuel temperature feedback is prompt and $\alpha_f < 0$. For BWR designs, the moderator density term in Eq. (31) is replaced by a term representing changes in the core average vapor fraction V_m:

$$\alpha_p \approx \frac{\partial \ln k}{\partial T_f}\frac{\partial T_f}{\partial P} + \frac{\partial \ln k}{\partial \ln V_m}\frac{\partial \ln V_m}{\partial P} \equiv \alpha_f \frac{\partial T_f}{\partial P} + \alpha_v \frac{\partial \ln V_m}{\partial P}, \quad (30)$$

where α_v is called the *void coefficient of reactivity*. We recognize that α_m and α_v are merely two different representations of the same moderator density effects on reactivity.

If there is a decrease in ρ_m caused by a power rise, thermal utilization f of Eq. (19) will increase because the number density of water and hence the thermal absorption cross section Σ_{a2}^M of moderator and Σ_{a2} decrease. This increase in f is, however, accompanied by a decrease in resonance escape probability p, since the water density reduction decreases the ability to slow down fast neutrons and hence decreases the slowing down cross section Σ_r. Neglecting small changes in the two remaining parameters, η and k_1, for k_∞ as well as in the nonleakage probability P_{NL} in Eq. (18), we note that the net effect of the moderator temperature and density changes in LWRs is determined by the competition between the conflicting changes in f and p. Thus, for some moderator density, a peak in k_∞ and k_{eff} will occur, as illustrated by a bell-shaped curve in Fig. 9. The left-hand half of the curve represents the under-moderated regime where water density does not allow optimal moderation of fast neutrons while the right-hand half corresponds to the over-moderated regime. In a typical LWR design, the rated operating condition is chosen somewhere in the under-moderated regime, as marked in Fig. 1, so that any increase in T_m or a decrease in ρ_m results in sliding down the k_{eff} curve. This implies that a PWR will have $\partial \ln k / \partial \rho_m > 0$ and hence $\alpha_m < 0$. Likewise, a BWR core operating in the under-moderated regime can guarantee $\alpha_v < 0$. Combined with the inherently negative value of α_f, negative values of α_m and α_v for PWRs and BWRs, respectively, always yield $\alpha_p < 0$, thus ensuring an automatic decrease in reactivity in the case of an inadvertent increase in power. Unfortunately, in the Chernobyl design, a positive value of α_v was possible at low power with a small number of control rods inserted, and that is where the 1986 accident was initiated. This clearly illustrates the importance of maintaining the proper design and operating parameters and, at the same time, should clarify the crucial point that a runaway power excursion is inherently impossible in any properly designed LWR plant.

Inherent Passive Safety Characteristics of Nuclear Reactors

This inherent safety characteristic of LWRs is extended further in LMR designs, where self-shutdown capability, even in the case of primary sodium pump failure coupled with a scram failure, was demonstrated (35) at the 20-MWe Experimental Breeder Reactor Unit II (EBR-II) in 1986. In this type of under-cooling event, the resulting power transient is sufficiently slow so that we may assume a quasi-static neutronic behavior and consider the net reactivity $\delta\rho \approx 0$ during the transient. Furthermore, the power transient primarily raises fuel temperature, while the sodium coolant temperature is determined largely by the flow coastdown rate. This allows us to represent the reactivity balance in terms of α_p decoupled from a coolant coefficient of reactivity α_c:

$$\delta\rho = \frac{\partial \ln k}{\partial T_f}\frac{\partial T_f}{\partial P}\delta P + \frac{\partial \ln k}{\partial T_c}\delta T_c \equiv \alpha_p \delta P + \alpha_c \delta T_c \approx 0. \quad (31)$$

Since both α_p and α_c are negative, an under-cooling transient can be terminated at a low power level corresponding to $\delta P < 0$, even with a scram failure, if $\delta T_c > 0$ results in an acceptable rise in sodium coolant temperature, which is exactly what was demonstrated succinctly in the EBR-II passive shutdown demonstrations.

The quasi-static analysis of Eq. (33) indicates that, to have the largest possible reduction in power, we desire to make α_p as small negative as feasible. This objective, however, should be contrasted with another objective we need to consider for a transient initiated by positive reactivity insertion $\delta\rho_{ex}$. With a quasi-static reactivity balance $\delta\rho = \delta\rho_{ex} + \alpha_p \delta P \approx 0$, in order to minimize the power increase δP, we need to maximize the magnitude of the negative α_p. This simple example illustrates that passive

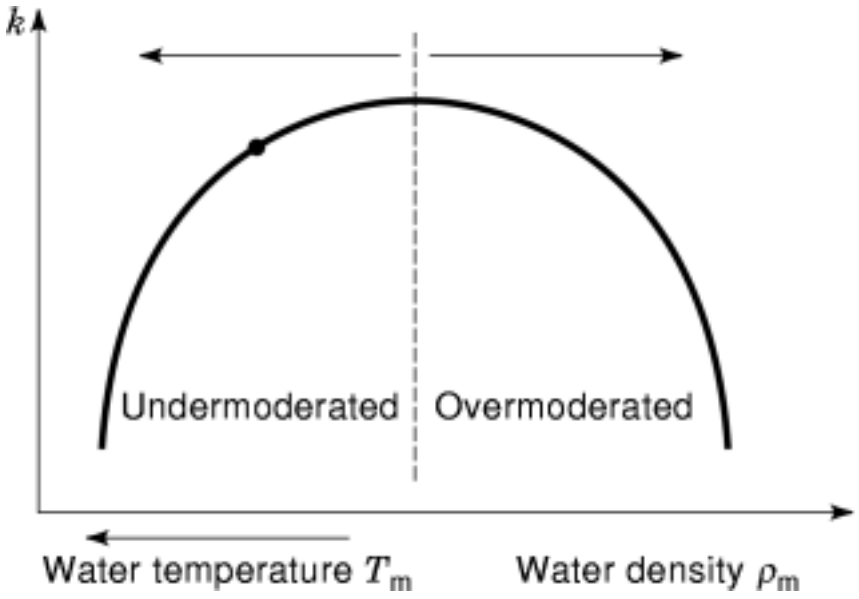

Figure 9. The effective multiplication factor k plotted as a function of coolant water density in an LWR core. The dot in the undermoderated regime indicates typical LWR operating conditions, illustrating the inherent safety feature that any inadvertent overheating of the coolant results automatically in a decrease in k and hence a reduction in power output.

safety of nuclear power plants requires a careful balance between a number of conflicting objectives. This perhaps is merely one of many challenges that lie ahead for nuclear engineers in developing the next generation of nuclear power plants.

NUMERICAL SOLUTION OF THE MGD EQUATIONS

Basic approach for solving the MGD equations entails standard finite-difference formulation (7) in each of the spatial dimensions represented. Since coupling between the groups, as indicated in Eqs. (14), is through the source terms on the RHS of the MGD equations, the numerical solution of the MGD equations can proceed group by group, with the source terms and core eigenvalue or k_{eff} iteratively updated in a *source* or *outer iteration*. Finite-difference solution of the MGD equations in one-dimensional geometry requires the inversion of a tri-diagonal matrix group by group. Inversion of the matrix is usually known as the *inner iteration*, although tri-diagonal matrices are usually inverted, without iteration, through the Gaussian elimination algorithm comprising the forward elimination and backward substitution steps. For two- and three-dimensional geometries, the inner iteration actually involves an iterative inversion of five- and seven-band matrices, respectively.

Although fine-mesh MGD calculations may be performed to yield a three-dimensional power distribution across individual fuel pins in a large nuclear reactor core, such calculations still require considerable computational resources and are usually reserved for benchmark problems. Routine reactor physics analysis often involves coarse-mesh MGD calculations, generically known as nodal calculations (36), coupled with pin-to-pin power distributions obtained from CP calculations, e.g., with the CASMO code. In the *nodal expansion method* (NEM), which forms the basis for the SIMULATE code (37), polynomial expansions approximate flux distributions within each node so that full-blown three-dimensional MGD solutions may be obtained with coarse spatial mesh. When the coarse-mesh NEM solution ϕ_{global} for the global flux distribution is combined with the intra-assembly solution ϕ_{form} to form the pin-to-pin flux distribution ϕ_{reactor}, discontinuities are encountered in ϕ_{reactor} at assembly boundaries. This is because two adjacent assemblies, with distinct fuel and control absorber arrangements, entail different intra-assembly flux distributions ϕ_{form}, and this would produce discontinuities in ϕ_{reactor} at the boundary between the assemblies, if ϕ_{global} is obtained to preserve the continuity of flux at each mesh boundary. To avoid discontinuities in ϕ_{reactor}, an *assembly discontinuity factor* (ADF) is calculated (38) as the ratio of the assembly-boundary flux to the assembly-average flux at each assembly boundary. The ADFs are applied to NEM calculations, as an interface flux condition, so that a discontinuity is induced in ϕ_{global} at each assembly boundary, which then offsets the differences in ϕ_{form} and renders ϕ_{reactor} continuous across assembly boundaries. The ADF approach, combined with global NEM and assembly CP calculations, allows us to reconstruct sufficiently accurate pin-to-pin power distributions for LWR core configurations with minimal computational requirements. Further development will be required to apply this type of synthesis approach to other core configurations, especially with non-square assembly geometry, and to time-dependent problems.

NEUTRON TRANSPORT THEORY AND COMPUTATIONAL ALGORITHMS

Although neutron diffusion theory provides many valuable insights to neutron behavior in a chain reacting system, we have recognized its limitation especially in representing material heterogeneities inherent at the unit-cell or assembly level. For this reason, we have discussed an integral from of the neutron transport equation in the CP lattice physics analysis. We now consider a full-blown integro-differential form of the neutron transport equation and discuss the important role it plays in reactor physics and

numerical algorithms developed to solve the equation. We extend the concept of neutron flux $\phi(\mathbf{r},t)$, which we now call the *scalar flux*, and define the *angular flux* $\psi(\mathbf{r},\Omega,t)$ in terms of the track length, similar to $\phi(\mathbf{r},t)$, but single out neutrons traveling in direction Ω. This allows us to interpret $\Omega\psi(\mathbf{r},\Omega,t)$ as the neutron current relative to a unit surface area normal to Ω and substitute it for $\mathbf{J}$ in the balance Equation (6). Adding the rate of neutrons scattered out of the energy interval of interest to the absorption rate to obtain the total collision rate and including the in-scattering rate of neutrons in the total source $S(\mathbf{r},\Omega,t)$, we obtain the *Boltzmann neutron transport equation*: (7, 39)

$$\frac{1}{\mathrm{v}}\frac{\partial\psi(\mathbf{r},\Omega,t)}{\partial t} = S(\mathbf{r},\Omega,t) - \nabla\cdot\Omega\psi(\mathbf{r},\Omega,t) - \Sigma\psi(\mathbf{r},\Omega,t), \quad (32)$$

where we suppress the energy dependence for notational convenience and $\Sigma = \Sigma_\mathrm{t}$. With the energy dependence included, the source term is given as an integral over both energy and directional variables, and Eq. (34) takes on the form of an integro-differential equation in seven variables: three in space, two in directions, energy, and time.

Numerical solution of the transport equation was the primary motivation behind J. von Neumann's effort to develop computing machines during the Manhattan Project and still remains a challenge for super-computers. Equation (34), slightly modified to represent the proper interaction mechanisms, also describes the transport of photons, i.e., γ- or x-rays, in radiation shielding and medical applications. Numerical solution of Eq. (34) for time-dependent transport problems is still in a rather limited stage of development but significant progresses have been made over the past three decades in solving the steady-state form of Eq. (34). Computational algorithms for solving the transport equation (34) can be classified as either deterministic or stochastic. Deterministic algorithms involve separation of variables techniques, discretization in the space of one or more variables, or a combination of both. Stochastic algorithms, often referred to as Monte Carlo algorithms, simulate a large number of neutrons undergoing collision and migration, and the mean behavior of the neutrons simulated yields the solution.

Deterministic Algorithms

We consider deterministic algorithms using a one-dimensional, steady-state form of Eq. (34) written in terms of μ, cosine of the angle θ between the direction of neutron motion and the spatial coordinate z:

$$\mu\frac{\partial\psi(z,\mu)}{\partial z} + \Sigma\psi(z,\mu) = S(z,\mu). \quad (33)$$

In a separation of variables technique, known as the P_n *method*, (7, 39) the angular flux $\psi(z,\mu)$, expanded as a function of Legendre polynomials $P_\mathrm{m}(\mu)$, is substituted into Eq. (35) and a coupled set of ordinary differential equations is obtained for the expansion coefficients $\phi_\mathrm{m}(z)$ by invoking the orthonormality properties of $P_\mathrm{m}(\mu)$. The set of differential equations is truncated by retaining the angular dependence of neutron population up to a certain order of anisotropy, i.e., by setting $\phi_\mathrm{m}(z) = 0$ for $m > n$. With the recognition that scalar flux $\phi(z) = \phi_0(z) = \int_{-1}^{1} d\mu\psi(z,\mu)$ and current $J(z) = \phi_1(z) = \int_{-1}^{1} d\mu\mu\psi(z,\mu)$, two equations for the P_1 approximation are identified as the diffusion Equation (6) and Fick's law of diffusion. The P_n equations are solved for $\phi_\mathrm{m}(z)$ through discretization schemes similar to those for the neutron diffusion equation.

Another approach to solve Eq. (35), called the S_n or *discrete ordinates method*, (38) entails calculating the angular flux for a few discrete values of μ and approximating the integral $\int_{-1}^{1} d\mu\psi(z,\mu)$ by a summation $\sum_n w_\mathrm{n}\psi(z,\mu_\mathrm{n})$ in terms of a suitable set of quadrature weights w_n. For discrete direction μ_n, approximating the derivative by a first-order difference over a mesh interval $\Delta z_\mathrm{j} = z_{\mathrm{j}+1/2} - z_{\mathrm{j}-1/2}$ yields

$$\mu_\mathrm{n}\frac{\psi(z_{\mathrm{j}+1/2},\mu_\mathrm{n}) - \psi(z_{\mathrm{j}-1/2},\mu_\mathrm{n})}{\Delta z_\mathrm{j}} + \Sigma\psi(z_\mathrm{j},\mu_\mathrm{n}) = S(z_\mathrm{j},\mu_\mathrm{n}), \quad (34)$$

where the cell-center flux $\psi(z_\mathrm{j},\mu_\mathrm{n})$ has to be obtained as a function of mesh-boundary fluxes $\psi(z_{j-1/2},\mu_n)$ and $\psi(z_{j+1/2},\mu_n)$. In the *diamond differencing* scheme, a simple arithmetic averaging is used: $\psi(z_\mathrm{j},\mu_\mathrm{n}) = 0.5\times[\psi(z_{j-1/2},\mu_n) + \psi(z_{j+1/2},\mu_n)]$. Given the source term $S(z_\mathrm{j},\mu_\mathrm{n})$, Eq. (36) is solved for mesh-boundary fluxes, following the direction of neutron travel for each μ_n. To avoid numerical difficulties, including negative values of flux, that are encountered in diamond differencing, a number of alternate high-order schemes have been developed. One popular scheme, called the *linear discontinuous* scheme, approximates $\psi(z,\mu_\mathrm{n})$ for each μ_n by a linear function which is discontinuous at the mesh boundaries. In this scheme, two difference equations, similar to Eq. (36), are solved for each spatial cell and for each discrete direction.

Once the angular flux $\psi(z,\mu_\mathrm{n})$ is solved through diamond differencing or alternative approaches, the source term $S(z_\mathrm{j},\mu_\mathrm{n})$ may be updated by using the latest estimate of $\psi(z,\mu_\mathrm{n})$ and the process repeated until convergence is reached. In this traditional source iteration method, the convergence can be slow, since the spectral radius ρ, i.e., the largest value of the magnitude of eigenvalues of the governing iteration matrix, is equal to the ratio $c = \Sigma_\mathrm{s}/\Sigma$. To overcome this difficulty, a number of alternate iteration schemes have been developed. In the *diffusion synthetic acceleration* (39, 40) scheme, the source iteration is accelerated by combining the discretized solution for $\psi(z,\mu_n)$ with a consistently discretized solution for a low-order approximation, usually diffusion theory or low-order P_n formulation. Significant accelerations can be attained in this synthetic approach, with the spectral radius ρ reduced to $0.23\,c$, for slab-geometry transport problems.

Monte Carlo Algorithms

By selecting a host of random numbers, Monte Carlo algorithms (38) simulate individual particles that follow physical laws of particle interaction and transport, as represented by Eq. (34), without the need to discretize any of the spatial, energy or direction variables. Monte Carlo algorithms offer the potential to provide accurate solutions for transport problems with complex geometries and material heterogeneities, with the solution accuracy limited only by the computing resources at our disposal. With rapid

advances made in computer hardware, there has been a significant increase in the popularity of Monte Carlo algorithms in both neutron and photon transport applications. This increased popularity owes in no small measure to the versatility that the MCNP5 code (41) offers: (1) simple description of complex geometries using well-defined surfaces, (2) separate or coupled neutron and gamma transport calculations, and (3) cross section libraries in continuous energy structure, rather than in discrete group formulation. Although the accuracy of Monte Carlo calculations is limited by the number of particle histories simulated, the MCNP code running on workstations provides acceptable accuracies for many practical calculations, especially for criticality calculations, where the eigenvalue is determined as a sum total of particle histories. Local flux or reaction rate calculations may, however, suffer from statistical fluctuations inherent in Monte Carlo calculations, especially in deep-penetration shielding problems.

ADVANCED REACTOR DESIGNS AND CHALLENGES FOR NUCLEAR ENGINEERS

In spite of proven safety records of LWR plants, both PWR and BWR, effort is continuing to develop new reactor and plant designs that reflect lessons learned from the current generation of power reactors. These advanced reactor designs cover a number of different features that may be classified as evolutionary in nature as well as those representing more radical changes and providing enhanced passive safety characteristics. For example, several power plants featuring two evolutionary LWR designs (42), ABB System 80+ and General Electric Advanced BWR (ABWR), have been operating in Korea and Japan, respectively, for past several years. Enhanced safety is clearly the focus of these new designs, which include improved ECCS features and an alternate emergency power source for System 80+ and installation of internal recirculation pumps for the ABWR. The elimination of external recirculation pumps, which are used in all BWR plants operating in the U.S., is expected to substantially reduce the likelihood of LOCAs in the ABWR.

One key example of advanced power plant designs is the AP1000 plant, which offers, with rated power of 1100 MWe, enhanced passive safety characteristics and competitive economics. The design includes passive features for safety injection of coolant during a LOCA, residual heat removal, and containment cooling. For example, cooling of the containment structure, both inside and outside, by natural circulation is effectively used. The design also features an increased size and hence a larger coolant inventory for the pressurizer and an increased reservoir of coolant through the in-containment refueling water storage tank. The AP1000 design received the final design certification (43) from the U.S. Nuclear Regulatory Commission in December 2005 and utility companies will be able to expedite the process of combined construction and operating license application with the certified design. The AP1000 design certification process required nearly two decades of development, starting with its predecessor AP600, and a cumulative expenditure of $600 million by Westinghouse Electric Company. The total generation cost, including capital, operating and maintenance, and fuel costs, is calculated to be $0.03−0.035/kWh of electricity for a twin-unit AP1000 plant.

Significant effort has been underway in the U. S. to develop a new breed of nuclear power plants, known as Generation IV plants, which could meet the demand for clean, economic electricity for the twenty-first century. The advanced reactor designs, including System 80+, ABWR, and AP600, are classified as Generation III plants, in contrast to Generation II plants comprising conventional PWR, BWR, and other plants operating currently in the U. S. and elsewhere. AP1000 is the first Generation III+ design to complete the design certification process. Other Generation III+ designs under development include General Electric Company's ESBWR (44) and Areva's USEPR designs (45), which offer power ratings around 1500 MWe. The Generation IV initiative (46) is built around innovative designs that will (a) increase economic competitiveness, (b) enhance safety and reliability, (c) minimize radioactive waste generation, and (d) increase nuclear proliferation resistance. Under the leadership of the U. S. Department of Energy (DOE), a multi-national study was performed to develop the Generation IV roadmap (46) and to select six most promising systems for detailed design and development. The DOE has selected to focus on the very-high temperature gas-cooled reactor (VHTR) and sodium-cooled fast reactor (SFR) designs for development in the U.S. among the six designs included in the roadmap. The VHTR design has the capacity to heat the helium coolant to temperatures in excess of 1100 K, suitable for the generation of hydrogen via dissociation of water. On the other hand, the SFR, operating with neutron energies around 0.1 MeV, offers the best potential for transmuting the entire transuranic elements, not just plutonium, from the LWR irradiated fuel inventory. In consideration of this potential, the DOE initiated in February 2006 the Global Nuclear Energy Partnership (GNEP) (47), which involves focused effort to develop SFR transmuters, together with the pyroprocessing and UREX+ aqueous processing technology (30, 31). The GNEP will actively pursue the reprocessing and recycling of LWR spent fuel, thereby significantly reducing the burden on the planned Yucca Mountain repository. The initiative also proposes that supplier nations, including the U.S., to provide slightly enriched LWR fuel to user nations, with the promise to take back spent fuel for reprocessing and recycling. This is a bold initiative that offers the potential to minimize the desire to develop indigenous uranium enrichment facilities in every country that would deploy nuclear power plants.

Incorporating advanced passive safety features in new innovative designs, the next generation of nuclear power plants is expected to be highly competitive in the world energy market. Realization of the goals enunciated for the Generation IV and GNEP initiatives will present new challenges to nuclear engineers. Power plant designs, including fuel, coolant, and engineered safety systems, should be optimized systematically. Many of design approaches and computer code packages need considerable updating and improvement, to increase the accuracy of design calculations in general and to accommodate passive safety features in particular. It has become increasingly neces-

sary to represent the dynamics of power plant systems in a fully integrated manner. This will require the development of efficient, verifiable super-system models in the near future. Similar challenges have to be met in the reactor physics arena. Improved fuel economics and increased dependence on reactivity coefficients for passive safety, especially for SFRs, demand substantial enhancement to the subgrid modeling and synthesis approaches, which characterize the reactor physics methodology in use today. Substantial effort will have to be made to improve and optimize the methodology for fuel management and operations support systems. Another challenge is the safe disposal of radioactive waste, even with Generation IV plants. This will require parallel effort to establish safe disposal sites and to successfully reprocess and recycle the entire transuranic materials via a synergistic use of LWR and SFR power plants.

U. S. nuclear power plants have achieved an impressive record of safe operation and low electricity generation cost in recent years, especially as a result of the formation of large operating companies owning as many as 20 nuclear plants each. Coupled together with the increasing need for clean, non-carbon-emitting energy around the world, there is considerable expectation that new Generation III+ plants will be ordered in 2007 or 2008, leading to successful deployment of Generation IV plants over the next 20–30 years.

CROSS-REFERENCES:

See (1) Fusion Reactors and (2) Nuclear Power Plant Design

BIBLIOGRAPHY

1. F. J. Rahn, A. G. Adamantiades, J. E. Kenton, and C. Braun, *A Guide to Nuclear Power Technology*, New York: Wiley, 1984.
2. R. A. Knief, *Nuclear Engineering*, 2nd ed., Washington: Hemisphere Publishing, 1992.
3. A. V. Nero Jr., *A Guidebook to Nuclear Reactors*, Berkeley, CA: University of California Press, 1979.
4. D. Testa (ed.), *The Westinghouse Pressurized Water Reactor Nuclear Power Plant*, Pittsburgh, PA: Westinghouse Electric Corporation, 1984.
5. R. L. Murray, *Nuclear Energy*, 4th ed., Oxford: Pergamon, 1993.
6. J. R. Lamarsh, *Introduction to Nuclear Engineering*, 2nd ed., Reading, MA: Addison-Wesley, 1983.
7. J. J. Duderstadt and L. J. Hamilton, *Nuclear Reactor Analysis*, New York: Wiley, 1976.
8. R. A. Serway, C. J. Moses, and C. A. Moyer, *Modern Physics*, Philadelphia: Saunders College Publishing, 1989.
9. J. G. Collier and G. F. Hewitt, *Introduction to Nuclear Power*, Washington, DC: Hemisphere Publishing, 1987.
10. N. J. McCormick, *Reliability and Risk Analysis*, Orlando, FL: Academic Press, 1981.
11. N. E. Todreas and M. S. Kazimi, *Nuclear Systems I: Thermal Hydraulic Fundamentals; II: Elements of Thermal Hydraulic Design*, New York: Hemisphere Publishing 1990.
12. H. Goldstein, *Fundamental Aspects of Reactor Shielding*, Reading, MA: Addison-Wesley, 1959.
13. *Reactor Physics Constants*, ANL-5800, 2nd ed., Argonne, IL: Argonne National Laboratory, 1963.
14. P. J. Turinsky, Overview of reactor physics calculations, InY. Ronen (ed.), *CRC Handbook of Nuclear Reactors Calculations*, Vol. III, 210–231, Boca Raton, FL: CRC Press, 1986.
15. S. F. Mughabghab, M. Divadeenam, and N. E. Holden, *Neutron Cross Sections, Vol. 1, Neutron Resonance Parameters and Thermal Cross Sections, Part A, Z = 1 − 60*, New York: Academic Press, 1981.
16. S. F. Mughabghab, *Neutron Cross Sections, Vol. 1, Neutron Resonance Parameters and Thermal Cross Sections, Part B, Z = 61 − 100*, Orlando, FL: Academic Press, 1984.
17. V. McLane, C. L. Dunford, and P. F. Rose, *Neutron Cross Sections, Vol. 2, Neutron Cross Section Curves*, San Diego, CA: Academic Press, 1988.
18. P. R. Rose (ed.), *ENDF/B-VI Summary Documentation*, ENDF-201, Upton, NY: Brookhaven National Laboratory, 1991.
19. P. J. Finck and C. Nordborg, The JEF evaluated data library—current status and future plans, *Trans. Am. Nucl. Soc.*, **73**: 422–424, 1995.
20. R. E. MacFarlane and D. W. Muir, *The NJOY Nuclear Data Processing System*, Version 91, LA-12740-M, Los Alamos: Los Alamos National Laboratory, 1994.
21. H. Henryson II, B. J. Toppel, and C. G. Stenberg, *MC^2-2:A Code to Calculate Fast Neutron Spectra and Multigroup Cross Section*, ANL-8144, Argonne, IL: Argonne National Laboratory, 1976.
22. L. E. Strawbridge and R. F. Barry, Criticality calculations for uniform water-moderated lattices, *Nucl. Sci. Eng.*, **23**: 58–73, 1965.
23. D. B. Jones, and K. E. Watkins, *CPM-3 Computer Code Manual*, EPR-CPM-001-M-002, Vol. 2, Rev. A, Palo Alto, CA: Electric Power Research Institute, 2000.
24. M. Edenius, K. Ekberg, B. H. Forssén, and D. Knott, *CASMO-4, A Fuel Assembly Burnup Program*, Studsvik/SOA-93/1, Newton, MA: Studsvik of America, 1993.
25. H. W. Graves Jr., *Nuclear Fuel Management*, New York: Wiley, 1979.
26. S. E. Aumeier, J. C. Lee, D. M. Cribley, and W. R. Martin, Cross-Section Parameterization Using Irradiation Time and Exposure for Global Depletion Analysis, *Nucl. Technol.*, **108**: 299–319, 1994.
27. *RELAP5/MOD3.3 Code Manual, Volume 1: Code Structure, Systems Models, and Solution Methods*, NUREG/CR-5535, Rev. 1, Washington, DC: U. S. Nuclear Regulatory Commission, 2001.
28. N. Tsoulfanidis and R. G. Cochran Radioactive Waste Management, *Nucl. Technol.*, **93**: 263–304, 1991.
29. N. C. Rasmussen, J. Buckham, T. J. Burke, G. R. Choppin, M. S. Coops, A. G. Croff, E. A. Evans, D. C. Hoffman, H. K. Forsen, G. Friedlander, B. J. Garrick, J. M. Googin, H. A. Grunder, L. C. Hebel, T. O. Hunter, W. M. Jacobi, M. S. Kazimi, C. J. King III, E. E. Kintner, R. A. Langley, J. C. Lee, G. E. Lucas, E. A. Mason, F. W. McLafferty, R. A. Osteryoung, T. H. Pigford, D. W. Reicher, J. E. Watson Jr., S. D. Wiltshire, and R. G. Wymer, *Nuclear Wastes: Technologies for Separations and Transmutation*, Washington, DC: National Academy Press, 1996.
30. J. J. Laidler, J. E. Battles, W. E. Miller, J. P. Ackerman, and E. L. Carls, Development of pyroprocessing technology, *Prog. Nucl. Energy*, **31**: 131–140, 1997.

31. G. F. Vandegrift, *et al.*," Lab-Scale Demonstration of the UREX+ Process,"Waste Management 2004 International Symposium, Tucson, AZ, 2004.
32. *Reactor Safety Study—An Assessment of Accident Risks in U.S. Commercial Nuclear Power Plants*, WASH-1400, Washington, DC: U.S. Nuclear Regulatory Commission, 1975.
33. *Severe Accident Risks: An Assessment for Five U.S. Nuclear Power Plants*, NUREG-1150, Vol. 1, Washington, DC: U.S. Nuclear Regulatory Commission, 1990.
34. G. F. Knoll, *Radiation Detection and Measurement*, 3rd ed., New York: Wiley, 2000.
35. H. P. Planchon, J. I. Sackett, G. H. Golden, and R. H. Sevy, Implications of the EBR-II inherent safety demonstration test, *Nucl. Eng. Design*, **101**: 75, 1987.
36. R. D. Lawrence, Progress in nodal methods for the solution of the neutron diffusion and transport equations, *Prog. Nucl. Energy*, **17**: 271–301, 1986.
37. K. S. Smith, *SIMULATE-3 Methodology, Advanced Three-Dimensional Two-Group Reactor Analysis Code*, Studsvik/SOA-92/02, Newton, MA: Studsvik of America, 1992.
38. K. S. Smith, Assembly homogenization techniques for light water reactor analysis, *Prog. Nucl. Energy*, **17**: 303–335, 1986.
39. E. E. Lewis and W. F. Miller Jr., *Computational Methods of Neutron Transport*, New York: Wiley, 1984.
40. E. W. Larsen, Diffusion-synthetic acceleration methods for discrete-ordinates problems, *Transport Theory Stat. Phys.*, **13**: 107, 1984.
41. F. B. Brown, *MCNP—A General Monte Carlo Code for N-Particle Transport Code*, Version 5, LA-UR-03-1987, Los Alamos, NM: Los Alamos National Laboratory, 2003.
42. E. L. Quinn," New nuclear generation–in our lifetime," *Nucl. News*, **52**,October 2001.
43. H. J. Bruschi," The Westinghouse's AP1000 affirmed by NRC," *Nucl. News*, **10**,February 2006.
44. D. Hinds and C. Maslak," Next-generation nuclear energy: The ESBWR," *Nucl. News*, **35**,January 2006.
45. R. C. Twilley, Jr.," EPR development – an evolutionary design process," *Nucl News*, **26**,April 2004.
46. "A Technology Roadmap for the Generation IV Nuclear Energy Systems," http://gif.inel.gov/roadmap, 2002.
47. "Global Nuclear Energy Partnership," http://www.gnep.energy.gov, 2006.

JOHN C. LEE
University of Michigan, Ann Arbor, MI